Author Manuscript

Author Manuscript

Author Manuscript

Author Manuscript

HHS Public Access

Author manuscript

Neurobiol Aging. Author manuscript; available in PMC 2021 August 01.

Published in final edited form as:

Neurobiol Aging. 2020 August ; 92: 114–134. doi:10.1016/j.neurobiolaging.2020.04.009.

Probiotics ameliorate intestinal pathophysiology in a mouse model of Alzheimer's disease

Harpreet Kaur[1], **Kumi Nagamoto-Combs**[2], **Svetlana Golovko**[1], **Mikhail Y Golovko**[1], **Marilyn G Klug**[3], **Colin Kelly Combs**[1,*]

[1]Department of Biomedical Sciences, University of North Dakota, School of Medicine and Health Sciences, 1301 N Columbia Road, Grand Forks, ND 58202-9037

[2]Department of Pathology, University of North Dakota, School of Medicine and Health Sciences, 1301 N Columbia Road, Grand Forks, ND 58203 USA 58202-9037

[3]Department of Population Health, University of North Dakota, School of Medicine & Health Sciences, 1301 N Columbia Road, Grand Forks, ND, 58203 USA 58202-9037

Abstract

Evidence suggests that changes in intestinal microbiota may not only influence gastrointestinal function but also affect the central nervous system (CNS). However, it is unclear whether alteration of the intestinal microbiota affects progression or inflammatory aspects of Alzheimer's disease (AD), one of the most common dementing neurodegenerative diseases. To understand the relationship of gut intestinal microbiota with AD pathology, wild type control (C57BL/6) mice were compared to a mouse line that has the human Aβ sequence knocked into the mouse APP gene ($App^{NL\text{-}G\text{-}F}$). In addition, we used probiotics to manipulate the gut microbiota of these animals. Fecal samples were collected to examine the overall diversity in intestinal microbiota. To study brain and intestinal inflammation, biochemical and histological analyses were performed. Altered metabolic pathways that could be associated with AD or the probiotic-mediated changes were examined by quantifying eicosanoid and bile acid profiles in brain and serum using ultra-performance liquid chromatography-tandem mass spectrometry (UPLC-MS/MS). We observed that brain pathology was associated with intestinal dysbiosis and increased intestinal inflammation and leakiness in the $App^{NL\text{-}G\text{-}F}$ mice. However, modulating gut bacteria using probiotics significantly decreased intestinal inflammation and gut permeability with minimal effect on plaque deposition, cytokine levels, or gliosis in the brain. Mass spectrometry data revealed altered levels of several bile acids and prostaglandins in serum as well as in brain due to AD or probiotic supplementation. Our study characterizes intestinal dysfunction in an Alzheimer's disease mouse model and the potential of probiotic intervention to ameliorate this condition.

*Corresponding author: Colin K. Combs colin.combs@und.edu.

Publisher's Disclaimer: This is a PDF file of an unedited manuscript that has been accepted for publication. As a service to our customers we are providing this early version of the manuscript. The manuscript will undergo copyediting, typesetting, and review of the resulting proof before it is published in its final form. Please note that during the production process errors may be discovered which could affect the content, and all legal disclaimers that apply to the journal pertain.

Disclosure

The authors have no actual or potential conflicts of interest.

Author Manuscript Author Manuscript Author Manuscript Author Manuscript

Keywords

Alzheimer's disease; *App*$^{NL\text{-}G\text{-}F}$ knock in mice; gut microbiome; probiotic VSL#3; intestinal inflammation; neuroinflammation; prostaglandins; bile acids

1. Introduction

The importance of the intestinal microbiome in health and disease has been documented with involvement in metabolism, nutrient absorption, immunomodulation, and numerous other physiologic functions (Guinane and Cotter, 2013; Jandhyala et al., 2015; Kau et al., 2011). The gut microbiota is comprised of microorganism species that live in the gastrointestinal tract and is the largest reservoir of microbes in the human body, containing about 10^{14} microbes (Sender et al., 2016). It has been demonstrated that the microbiome is quite stable in healthy adults. However, it can be influenced by long term stimuli such as changes in diet, physical activity, illness/infection, or drug therapies like antibiotic treatment (Gerber, 2014). Dysbiosis or alteration in the composition of gut microbiota has been related to an increasing number of intestinal and extra-intestinal diseases including irritable bowel syndrome (IBS), celiac disease, allergy, asthma, metabolic syndrome, cardiovascular disease, and obesity (Carding et al., 2015). There is emerging evidence that changes in intestinal bacterial composition can affect a wide range of neurological and neurodevelopmental conditions including autism (Finegold et al., 2010), depression (Evrensel and Ceylan, 2015), schizophrenia (Nguyen et al., 2018), and multiple sclerosis (Chen et al., 2016) through a gut-brain axis. However, a functional link between gut bacteria and neurodegenerative diseases such as Alzheimer's disease (AD) remains less explored.

AD is a common form of age-related dementia with incidence approaching 30% in people over the age of 85 and is considered one of the major causes of death in the elderly (Lopez et al., 2013; Qiu and Fratiglioni, 2018). A neuropathological hallmark of Alzheimer's disease is accumulation of amyloid plaques in the brain which are known to be associated with elevated levels of inflammatory mediators (Morales et al., 2014). Although AD is commonly considered a central nervous system disease, there is evidence that peripheral organs may be affected (Aderem and Underhill, 1999; Adriani et al., 2014; Joachim et al., 1989; Puig et al., 2015; Semar et al., 2013). Indeed, our recent work in both a transgenic mouse model of AD and human AD colons demonstrated increased β-amyloid (Aβ) immunoreactivity and phospho-tau changes not unlike changes that occur in the brain (Puig et al., 2015). This suggests that the enteric nervous system, in addition to the central nervous system, may be affected during disease supporting a gut-brain axis pathophysiology.

In support of this idea, there has been growing interest in understanding how alterations in the gut microbiota can be associated with memory impairment and onset of Alzheimer disease (Austin and Combs, 2010; Pistollato et al., 2016; Wu et al., 2017). A recent study by Harach *et al.,* using APP/PS1 transgenic mice indicated microbial involvement in the development of Aβ pathology (Harach et al., 2017). Other studies also suggest an association between differential microbial composition and AD pathology (Balin et al., 2008; Dinan et al., 2015; Vogt et al., 2017). Additionally, a probiotic, *Lactobacillus*

Author Manuscript Author Manuscript Author Manuscript Author Manuscript

plantarum, has been documented to be beneficial in a rat model of AD by restoring acetylcholine levels and ameliorating cognitive deficits (Nimgampalle and Kuna, 2017). Probiotics *Bifidobacterium longum* and *Lactobacillus acidophilus,* in combination with exercise, decreases the number and area of amyloid plaques in the hippocampus of an AD mouse model (Arai et al., 1991). A positive effect of probiotic consumption on improvement in some oxidative stress and inflammatory markers has been observed in AD patients supporting a gut-brain communication during disease (Akbari et al., 2016). However, others report that modifying gut bacteria in humans with probiotic supplementation provided no change in cognitive functions or inflammation in severe AD patients (Arendash et al., 2001).

These studies indicate that changes in intestinal microbiota may have effects on the brain to influence disease progression. However, there has been little work done to determine whether there exists an intestinal pathophysiology in AD and, if so, how changes in microbiome may be contributing to or attenuating this aspect of the disease. Therefore, this study was conducted to ask the straightforward question of whether AD manifests with intestinal presentation using the $App^{NL\text{-}G\text{-}F}$ mouse model of disease. In the $App^{NL\text{-}G\text{-}F}$ mouse model, APP is not overexpressed but levels of pathogenic Aβ are elevated due to the combined effects of three mutations (Swedish “NL”, the Iberian “F”, and the Arctic “G” mutations) associated with familial AD (Saito et al., 2014). As expected, we observed a robust, disease-associated increase in intestinal inflammatory state and permeability. In order to investigate whether the observed dysfunctions were due to intestinal dysbiosis, we quantified fecal bacterial composition, bile acid, and prostaglandin profiles in diseased mice and assessed any changes in intestinal phenotype following supplementation with the probiotic medical food mixture, VSL#3. VSL#3 is a commercially available probiotic cocktail, consisting of eight strains of lactic acid-producing bacteria. As predicted, probiotic supplementation improved intestinal dysfunction. However, the benefits were surprisingly limited to the intestines with little effect on Aβ plaque load or gliosis. This supports a compelling premise that dysbiosis-mediated intestinal dysfunction is a significant manifestation of disease outside of the brain. More importantly, our findings indicate that a gut-targeted probiotic feeding intervention can provide significant benefits towards intestinal aspects of disease that do not communicate effectively to the brain. This suggests increased complexity of the mechanisms of gut-brain communication during disease.

2. Materials and Methods

2.1 Animals

$App^{NL\text{-}G\text{-}F}$ mice were obtained from Dr. Takaomi C. Saido, Laboratory for Proteolytic Neuroscience, RIKEN Center for Brain Science, Japan. APP is not overexpressed in $App^{NL\text{-}G\text{-}F}$ mice but levels of pathogenic Aβ are elevated due to effects from three mutations associated with familial AD. Specifically, an APP construct containing a humanized Aβ region, includes the Swedish “NL”, the Iberian “F”, and the Arctic “G” mutations was used (Saito et al., 2014). This model was selected to avoid potential artifacts introduced by APP over-expression. Thirty $App^{NL\text{-}G\text{-}F}$ and 30 C57BL/6 (wild type) control female mice in total were used at 6-8 months of age. From this pool of 30, different numbers of mice were used for each analysis as described in each figure legend. Our earlier work with $App^{NL\text{-}G\text{-}F}$ line

Author Manuscript Author Manuscript Author Manuscript Author Manuscript

demonstrated similar Aβ deposition and gliosis across sex with a more robust behavior phenotype in females (Manocha et al., 2019). Based upon this, we elected to use female mice in the initial study but recognize that future work requires a comparison of probiotic effects on both male and female mice. We elected to use the *App*$^{NL\text{-}G\text{-}F}$ mice at 6-8 months of age simply to select a time when extensive plaque deposition and gliosis occurred to provide a high background for any ameliorative benefits the probiotic might provide. These mice develop plaques at the age of 2 months with saturation around 7 months (Saito et al., 2014). Our C57BL/6 mice were from an in-house colony originally obtained from Jackson Laboratories. Upon receiving the *App*$^{NL\text{-}G\text{-}F}$ mice they were bred with the in-house C57BL/6 mice but were ultimately maintained as a homozygous colony. Therefore, although both lines are from established in-house homozygous colonies, they were not littermate controls. Although internal reports from Jackson Laboratories indicates little substrain differences between C57BL/6J and C57BL/6N mice regarding fecal microbial structure there are significant differences across vendors (https://www.jax.org/news-and-insights/jax-blog/2019/august/microbiome-stability). However, as expected from prior work, we anticipate that recognized institutional drift in fecal microbiome composition will have normalized the *App*$^{NL\text{-}G\text{-}F}$ to the wild type mice to our husbandry conditions (Montonye et al., 2018). Animal use was approved by the University of North Dakota Institutional Animal Care and Use Committee (IACUC) protocol. The animals were provided food and water *ad libitum* and housed with a 12-h light/dark cycle.

2.2 Animal groups and probiotic (VSL#3) dosing

Animals were randomly assigned into four groups: 1) wild type supplemented with vehicle (WT Veh), 2) wild type supplemented with VSL#3 (WT VSL), 3) *App*$^{NL\text{-}G\text{-}F}$ supplemented with vehicle (*App*$^{NL\text{-}G\text{-}F}$ veh), and 4) *App*$^{NL\text{-}G\text{-}F}$ supplemented with VSL#3 (*App*$^{NL\text{-}G\text{-}F}$ VSL#3) and were fed normal pelleted Envigo-Harlan Teklad 22/5 rodent diet, 8640. The vehicle used was MediGel® (Clear H_2O, Portland, ME, USA), and VSL#3 was dissolved in the vehicle and administered to animals daily at estimated mean water consumption at 5 mL/25g mouse/day. The treatment was given for eight weeks and the dose of probiotic VSL#3 (0.32×10^9 CFU bacteria/25g mice) was calculated based on the body surface area normalization method from the recommended human dose of VSL#3 (Chan et al., 2016; Reagan-Shaw et al., 2008). As per the manufacturer recommendation, human colonization takes place in 2-3 weeks and we elected a longer time period of 8 weeks based upon known resistance of mice to probiotic colonization (Zmora et al., 2018). VSL#3 is a commercially available probiotic cocktail (Leadiant Biosciences, Inc., Gaithersburg, MD, USA) of eight strains of lactic acid-producing bacteria: *Lactobacillus plantarum, Lactobacillus delbrueckii subsp. Bulgaricus, Lactobacillus paracasei, Lactobacillus acidophilus, Bifidobacterium breve, Bifidobacterium longum, Bifidobacterium infantis, and Streptococcus salivarius subsp. Thermophilus.* VSL#3 is a well-known medical food that has been shown to improve disease symptoms in the treatment of ulcerative colitis and pouchitis, an inflammation of the ileal pouch in colectomy patients, liver cirrhosis and hepatic encephalopathy (Dhiman et al., 2014; Tursi et al., 2010).

Author Manuscript Author Manuscript Author Manuscript Author Manuscript

2.3 Antibodies and reagents

FITC-dextran (MilliporeSigma, Burlington, MA, USA), ELISA kits for TNF-α, IL-1β, IL-10, and lipocalin were purchased from R&D Systems (Minneapolis, MN, USA). Antibodies against GFAP, Aβ, BACE-1, and PSD-95 were purchased from Cell Signaling Technology Inc. (Danvers, MA, USA). Anti-synaptophysin, anti-synapsin 1, anti-cFos, and anti-COX-2 antibodies were purchased from Abcam (Cambridge, MA, USA). Anti-Iba-1 antibody was purchased from Wako Chemicals USA, Inc. (Richmond, VA, USA). iNOS antibody was purchased from BD, Biosciences (San Jose, CA, USA). Anti-GAPDH, α-tubulin antibodies and horseradish peroxidase-conjugated secondary antibodies (goat anti-mouse IgM, goat anti-mouse IgG, goat anti-rabbit, goat anti-rat, bovine anti-goat and bovine anti-mouse were purchased from Santa Cruz Biotechnology (Santa Cruz, CA, USA). Elite Vectastain ABC reagents, Vector VIP, biotinylated anti-rabbit, and anti-mouse antibodies were purchased from Vector Laboratories Inc (Burlingame, CA, USA). Standards used in mass spectroscopy analysis were purchased from MilliporeSigma (Burlington, MA, USA). Autosampler vials were obtained from ThermoFisher Scientific, (Waltham, MA, USA), silanized micro-vial inserts were from Agilent (Santa Clara CA; part #5181-8872) and inserts were from VWR (Radnor, PA, USA).

2.4 Fecal sample collection and microbiome analysis

After 8 weeks of probiotic treatment, fecal samples were obtained by placing each mouse separately in a clean cage for 10-30 min and fecal pellets were collected in a sterile 1.5 mL Eppendorf tube. More than 90% of the mice excreted a fecal pellet within one min of being placed into a clean cage. In those instances, in which a mouse did not pass stool within 30 mins, the mouse was gently picked up vertically by the tail for 20-30 seconds until a stool pellet was excreted and collected. Samples were stored at 4°C until all samples were collected and later stored at −80°C until microbiome analysis. The fecal samples were sent to RTL Genomics (Research and Testing Laboratory, Lubbock, TX, USA) for 16S rRNA sequencing. Hypervariable regions V1 to V3 of 16S rRNA gene were amplified for sequencing at RTL Genomics in a reaction using Hot-Start Taq Master Mix Kit (Qiagen, Inc., Germantown, MD, USA) with the universal primer set 27F/519R. The sequence data were analyzed using a standard microbial diversity analysis pipeline, which consisted of two major stages, denoising and chimera detection followed by microbial diversity analysis. The overall diversity (which is determined by both richness and evenness, the distribution of abundance among distinct taxa) was studied following 8 weeks of treatment. The number of different species or species richness in each experimental group was studied using chao index. Shannon diversity is commonly used to characterize the abundance and evenness of the species present in a community and was used as an index of evenness in this study. Measures of diversity were screened for group differences using two-way analysis of variance (ANOVA).

2.5 Intestinal permeability

In vivo intestinal permeability was measured to assess barrier function by determining the amount of FITC-dextran in the blood after it was orally administered as described previously (Zakostelska et al., 2011). Briefly, food and water were withdrawn for 2 h and mice were

Author Manuscript Author Manuscript Author Manuscript Author Manuscript

orally gavaged with the permeability tracer (484 mg/kg body weight of FITC-labeled dextran, 4.4kDa, MilliporeSigma). As mentioned, blood was collected 5 hours post-gavage during animal sacrifice and centrifuged at 7,168 g for 10 min to obtain serum. The fluorescence intensity was read in the serum using a BioTek FLx800 fluorescence plate reader (excitation, 492 nm; emission, 525 nm) with Gen5 v3.02 software (BioTek Instruments, Winooski, VT, USA). FITC-dextran concentrations were determined using a standard curve generated by serial dilutions of FITC-dextran.

2.6 Gastric emptying and intestinal geometric center (intestinal transit)

Gastric emptying and intestinal transit were determined by assessing the distribution of a 70 kDa FITC conjugated dextran marker (70 kDa FITC-dextran; MilliporeSigma) throughout the gastrointestinal tract of mice as described previously (Aube et al., 2006). To perform this experiment, mice were fasted 10 hours then given 100 μL of FITC dextran (8.3 mg) via oral gavage and intestines were collected 30 min later. To access intestinal motility, the stomach (segment 1) and the small intestines (divided into equal 8 segments 2-9) were flushed with PBS and washes were collected. Intestinal washes were centrifuged 16,128g for 5 min and the fluorescence of supernatant was measured using a fluorescence plate reader (excitation, 492 nm; emission, 525 nm). Fasting for longer periods in rats has previously demonstrated no effect on basal gastric emptying (Brito et al., 2015).

Gastric emptying was measured by subtracting FITC-dextran remaining in the stomach from total dextran (in small intestine and stomach) and dividing this by total dextran. To get the percentage of gastric emptying, the value obtained was multiplied by 100. Intestinal transit was analyzed using the intestinal geometric center (IGC) of the distribution of dextran throughout the intestine and was calculated following the equation described by Miller and colleagues (Andreasson et al., 2016).

$$IGC = \Sigma[(fraction\ of\ amount\ of\ FITC in\ each\ segment) \times (segment\ number)]$$

Or

$$IGC = \Sigma_{n=1}^{N} FITC_n \times n$$

where N is total number of segments, $FITC_n$ is fraction amount of FITC in each segment and n is the segment number.

2.7 Enzyme Linked Immunosorbent Assay (ELISA) for Aβ and cytokines

Following the eight-weeks treatment paradigm, the animals were euthanized via CO_2 asphyxiation followed by cervical dislocation and cardiac exsanguination. The brains and ileums of each animal were collected for biochemical as well as histological procedures. Right temporal cortices and ileums of the small intestines (after rinsing out contents) were collected and flash frozen in liquid nitrogen and stored at −80 °C for subsequent use. A small part of the flash frozen ileums and temporal cortices were weighed and lysed in ice cold radioimmunoprecipitation assay buffer (RIPA) buffer (20 mM Tris, pH 7.4, 150 mM

Author Manuscript Author Manuscript Author Manuscript Author Manuscript

NaCl, 1 mM Na_3VO_4, 10mM NaF, 1 Mm EDTA, 1 mM EGTA, 0.2 mM phenylmethylsulfonyl fluoride, 1% Triton, 0.1% SDS, and 0.5% deoxycholate) with protease inhibitors (AEBSF 1 mM, aprotinin 0.8 μ M, leupeptin 21 μM, bestatin 36 μM, pepstatin A 15 μM, E-64 14 μM). Additional DNase was added to digest DNA in the ileum samples. The samples were mechanically homogenized using beads in a Bullet Blender Storm homogenizer 24 (Next Advance, Inc. Troy, NY, USA) and later centrifuged to remove the insoluble content. The resulting tissue lysates (supernatant) from temporal cortices and ileums were used for soluble Aβ 1-40 and Aβ 1-42 ELISAs. The pellet or insoluble content was re-suspended in 5M guanidine HCl/50 mM Tris HCl, pH 8.0 and samples were again bullet blended and centrifuged (21,000 g, 4°C, 10 min) and the supernatant was removed and used to determine insoluble Aβ concentrations (Aβ 1-40 and Aβ 1-42 ELISA). The levels of soluble and insoluble Aβ 1-40 and Aβ 1-42 were quantified using commercially available ELISA kits from MilliporeSigma. The levels of Aβ 1-40 and Aβ 1-42 (soluble and insoluble) were reported as pg/mL per mg protein derived from a standard curve establish for each protein. Protein concentrations of cell lysates were determined using the bicinchoninic acid (BCA) protein determination assay (ThermoFisher Scientific).

For cytokines analyses, a portion of the flash frozen intestine as well as brain samples were homogenized in 1X PBS containing protease inhibitors using a bullet blender at medium speed followed by centrifugation at 21,000 g for 10 min. The levels of proinflammatory cytokines (TNF-α, IL-1β and IL-6) and the proinflammatory marker protein, lipocalin, were measured from the supernatants using commercially available ELISA kits (R&D Systems). Total protein concentrations were assessed using the BCA assay and equal amounts of protein were added per ELISA well. The results are expressed as pg/mL per mg of protein.

2.8 Western blot analysis

A portion of the flash frozen temporal cortices and ileums were prepared in RIPA buffer containing protease inhibitors and bullet blended and centrifuged (21,000 g, 4°C, 10 min) to remove insoluble content. DNase (50U/mL DNAse1) was added to RIPA buffer in ileum samples preparation. Protein content of the cell lysates was determined using BCA protein determination assay (Pierce Biotechnology, Rockford, IL, USA). The resultant supernatants were boiled in sodium dodecyl sulfate (SDS) containing gel-loading sample buffer for 5 mins. 15 μg of each total protein extract was resolved on a 10% SDS polyacrylamide gel. Separated proteins were transferred onto polyvinylidene difluoride membranes (PVDF) for western blotting using anti-APP, BACE 1, GFAP, Iba-1, COX-2, PSD-95, synaptophysin, synapsin 1, iNOS, cFos, occludin, GAPDH (loading control), and α-tubulin (loading control) antibodies. Bands were visualized using enhanced chemiluminescence (GE Healthcare, Piscataway, NJ). Chemiluminescence images were captured using an Aplegen Omega Lum G imaging system. Optical densities were quantified using Adobe Photoshop 12.0 software. Optical density values were normalized to the relevant loading control GAPDH/α-tubulin optical density values from the same membrane.

2.9 Eicosanoid analysis

Blood samples collected at the time of sacrifice were allowed to rest for 60 min at room temperature and centrifuged at 7,168 g for 10 min to obtain serum. Serum eicosanoids were

Author Manuscript Author Manuscript Author Manuscript Author Manuscript

extracted using a one-step extraction with methanol as we previously described with minor modifications (Brose, S.A. et al., 2013). Briefly, 20 μL of serum were mixed with 60 μL of 100% methanol containing 1 ng of PGE2-d9 and 10 ng of 20:4n-6-d8 (Cayman Chemicals, Ann Arbor, MI) as internal standards. For temporal cortex eicosanoid analysis, ~20 mg of flash frozen tissue was mixed with 100 μL of 100% methanol containing the same amounts of internal standards. After spinning at 12,000g for 10 min, supernatants were transferred to silanized micro-vial inserts and analyzed using UPLC-MS/MS as we previously described (Golovko and Murphy, 2008). LC separation was performed on a Waters ACUITY UPLC HSS T3 column (1.8 μM, 100 Å pore diameter, 2.1×150mm, Waters, Milford, MA, USA) with an ACUITY UPLC HSS T3 precolumn (1.8 μM, 100 Å pore diameter, 2.1x5mm, Waters) at a temperature of 55°C. The LC system consisted of a Waters ACUITY UPLC pump with a well plate autosampler at 8 °C. Ten microliters of sample were injected on column.

For UPLC separation we used our previously described method (Brose, S.A. et al., 2013). Solvent A consisted of water containing 0.1% formic acid and solvent B consisted of acetonitrile with 0.1% formic acid. The flow rate was maintained at 0.45 mL/min. Solvent B was held at 39% B for 0.5 min, then increased to 40.5% over 6.88 min, to 70% over 1.62 min, to 75% over 3 min, and further increased to 98 over 1.5 min where it was held for 5.3 min. For column re-equilibration, solvent B was returned to initial conditions over 0.2 mins and hold at 39% for 2 min before next sample injection.

Eicosanoids and 20:4n-6 were analyzed using a triple quadrupole mass spectrometer (Xevo TQ-S, Waters) with electrospray ionization operated in negative ion mode. The capillary voltage was 2.35 kV and the cone voltage was 30V. The desolvation temperature was 550 °C and the source temperature was 150 °C. The desolvation gas flow was 1000 L/hr, the cone gas flow was 150 L/hr, and the nebulizer gas was at 7.0 Bar. MassLynx V4.1 software (Waters) was used for instrument control, acquisition, and sample analysis.

All eicosanoids were quantified against PGE2-d9, and 20:4n-6 was quantified using 20:4n6-d8, as internal standards. The deuterated PGE2 has been previously validated as an internal standard for all PG analyzed (Marksteiner et al., 2018). The analytes were monitored in MRM mode as previously described (Brose and Golovko, 2012) with the following mass transitions: PGE2 - 351.18/271.13; PGD2 - 351.06/271.14; 6-ketoPGF1α - 369.26/163.07; PGF2α - 353.07/193.04; TXB2 - 369.20/169.00; 20:4n6 - 303.07/259.21; PGE2-d9 - 360.2042/280.17. The collision energies used were (V): PGE2 - 16; PGD2 - 16; 6-ketoPGF1α - 24; PGF2α - 20; TXB2 - 12; PGE2-d9 - 16; 20:4n6 - 12; 20:4n6-d8 –12.

2.10 Bile acid analysis

Bile acids from serum and flash frozen cortical samples were separated from proteins by mixing with methanol containing bile acid deuterium labeled standards (1 ng of taurocholic-d_5, cholic-d_4, glycocholic-d_4, and 10 ng of chenodeoxycholic-d_4, Medical Isotopes, Pelham, NH). We used 20 μL of serum mixed with 60 μL of 100% methanol, and ~20 mg of cortex mixed with 100 μL of 100% methanol. After spinning at 12,000g for 10 min, supernatants were transferred to silanized microvial inserts and analyzed using UPLC-MS/MS in the selected reaction monitoring and selected ion monitoring modes.

Author Manuscript Author Manuscript Author Manuscript Author Manuscript

UPLC separation was performed on a Waters ACUITY UPLC HSS T3 column (1.8μM, 100 Å pore diameter, 2.1x150mm, Waters, Milford, MA) with an ACUITY UPLC HSS T3 pre-column (1.8 μM, 100 Å pore diameter, 2.1x5mm, Waters) at a temperature of 55°C using a previously described method (Brose, S. et al., 2013). The LC system consisted of a Waters ACUITY UPLC pump with a well plate autosampler at 8 °C. Ten microliters of sample were injected on column. Solvent A was water containing 0.1% formic acid and solvent B was acetonitrile with 0.1% formic acid. The flow rate was maintained at 0.45 mL/min. Bile acids were eluted with increasing gradient of solvent B from 39% B 98% as we previously described (Brose, S. et al., 2013).

Bile acids were analyzed using a triple quadrupole mass spectrometer (Xevo TQ-S, Waters) with electrospray ionization operated in negative ion mode. MassLynx V4.1 software (Waters) was used for instrument control, acquisition, and sample analysis. All bile acids were quantified against deuterium labeled internal standards using selected ion monitoring tracers. Reaction monitoring tracers were used for analyte confirmation. Tauro-cholic (Finegold et al.), tauro-α-muricholic (TαMC), tauro-ω-muricholic (TωMC), tauro-β-muricholic (TβMC), taurodeoxycholic (TDC), taurochenodeoxycholic (TCDC) were quantified against TC-d_5; glycocholic (GC) and glycolchenodeoxycholic (GCDC) were quantified against GC-d_4; cholic (C), α-muricholic (αMC), ω-muricholic (ωMC), and β-muricholic (βMC) were quantified against C-d_4; deoxycholic (Zakostelska et al.), chenodeoxycholic (CDC), and litocholic (Finegold et al.) were quantified against CDC-d_4.

The following mass transitions (with collision energies indicated in parentheses (V)) were used: TC, TαMC, and TωMC 514.40/123.90 (48); TC-d_5 519.30/123.90 (48); TDC 498.32/123.91 (46); TCDC 498.29/123.91 (50); GC 464.30/402.12 (32); GCDC 448.30/386.40 (42); GC-d_4 468.32/406.12 (32); C, αMC, βMC, and ωMC 407.31/343.18 (30); C-d_4 411.33/346.96 (32); DC, CDC, and LC 391.29/373.17 (34); CDC-d_4 395.26/377.30 (34).

2.12 Immunohistochemistry

Following the eight-week treatment paradigm the left brain hemisphere of each animal was fixed in 4% paraformaldehyde and prepared for histologic analysis as described previously (Nagamoto-Combs et al., 2016). Briefly, paraformaldehyde-fixed tissue was embedded in a 15% gelatin (in 0.1 M phosphate buffer) matrix and immersed in a 4% paraformaldehyde solution for 2 days to harden the gelatin matrix followed by two changes of 30 % sucrose for cryoprotection for two days each. The blocks were then flash frozen using dry ice/isomethylpentane, and 40μm serial sections were cut using a freezing microtome. Serial sections of 40μm were cut and stored at 4°C in PBS with 0.1% sodium azide until immunostaining. Anti-Aβ (1:1000), anti-GFAP (1:700), anti-Iba-1 (1:750) antibodies were used for immunodetection in sections followed by incubation with biotinylated secondary antibodies (1:2000 dilution; Vector Laboratories) and an avidin/biotin complex (Vector ABC kit). Immunoreactivity was visualized using Vector VIP as the chromogen. The stained sections were mounted onto gelatin-coated slides and coverslipped using VectaMount (Vector Laboratories) following a standard dehydrating procedure through a series of ethanol concentrations and Histo-Clear (National Diagnostics, Atlanta, GA, USA). A Leica

Author Manuscript Author Manuscript Author Manuscript Author Manuscript

DM1000 microscope and Leica DF320 digital camera system (Leica Microsystems Inc., Buffalo Grove, IL, USA) were used to take images and quantification of immunostaining was performed as described previously (Dhawan and Combs, 2012). Briefly, optical densities from the temporal cortex from the same serial sections were measured using Adobe Photoshop software (Adobe Systems). The values for each section were averaged (3 sections/brain, 6-7 brains per condition) and plotted.

2.13. Behavior test (Cross Maze)

Cross maze testing was performed to assess the working memory of WT and $App^{NL\text{-}G\text{-}F}$ animals. The maze consisted of four arms 30 cm long and 5 cm wide each arranged in a cross configuration with a central 5 cm square area. Each arm had a 15 cm high wall along each side and at the end and the central area of the maze was open for the duration of the session. Mice were tested following the 8 weeks of VSL#3 supplementation. Each animal was placed gently at a starting point at the end of one arm (constant for each animal) and allowed to explore the maze freely for 10 min. The order of arm choices made by each animal was recorded using a video camera mounted above the center of the maze and analyzed using ANYmaze software (Stoelting Co., Wood Dale, IL). A correct alternation is defined as visiting each of the four arms without re-visiting any arm. The number of alternations were counted (defined as 4 consecutive entries into 4 different arms), and % alternation for each mouse was calculated as follows: # alternations/(total entries-3). The mice that made fewer than 12 choices in an alternation task were excluded from the analysis. Mice were returned to their home cages following completion of behavior testing.

2.14 Statistical analysis

Statistical analyses were performed using IBM SPSS, version 26.0 (IBM SPSS Statistics for Windows, Version 26.0. Armonk, NY: IBM Corp) employing two-way and one-way ANOVA or Kruskall-Wallis test. The tests for outliers (Grubb's Single Outlier test and Rosner's ESD Many Outlier test) and normality (Shapiro-Wilk W, Anderson-Darling, Martinez-Inglewicz, Kolomogorov-Smirnov, and D'Agostino Skewness, Kurtosis, and Omnibus) were done using NCSS 12 (NCSS 12 Statistical Software (2018). NCSS, LLC. Kaysville, Utah, USA, ncss.com/software/ncss). If the data followed a normal distribution, two-way or one-way ANOVA were performed, as appropriate, to assess differences between genotypes followed by a Tukey-HSD post-hoc test for performing multiple comparisons between the studied groups (genotypes and treatments). If the data was not normally distributed, the Kruskall-Wallis test was performed to assess statistical significance. The results are presented as mean ± S.E.M. Differences were considered significant when $p<0.05$. All the plots given in the manuscript were made using GraphPad software (Prism version 7.00 for Windows, GraphPad Software, La Jolla California USA).

3. Results

3.1 Fecal bacterial community composition differed between WT control and AD mice and was affected by VSL#3 feeding

To determine whether differences in intestinal microbiome were a component of AD pathophysiology, we studied bacterial diversity (Shannon Diversity index) and species

Author Manuscript Author Manuscript Author Manuscript Author Manuscript

richness (Chao 1 index) in fecal samples of C57BL/6 (WT) and App^{NL-G-F} (AD) mice with and without eight weeks of dietary supplementation with VSL#3. Although there were no differences between vehicle groups (WT veh and App^{NL-G-F} veh mice), App^{NL-G-F} mice fed VSL#3 had a significant increase in both species richness and bacterial diversity (Fig. 1a, b) which shows that probiotic supplementation improved (enhanced) both the different number of microbial species (richness) and also increased the diversity of microbial species (evenness) in animals. Beta diversity plotted in form of principle coordinate analysis (PCoA) showed distinct cluster between WT and App^{NL-G-F} mice (Fig. 1c). The relative abundance of different phyla was quantified to demonstrate significant differences (Fig. 1d). The ratio of the two most abundant phyla, Firmicutes and Bacteroidetes, was different across genotypes (WT and App^{NL-G-F}). An increase in abundance of Bacteroidetes and decreased abundance of Firmicutes was observed in App^{NL-G-F} mice when compared to WT controls (Fig. 1e). No significant difference was observed in other phyla (Proteobacteria, Verrucomicrobia, Actinobacteria, Deferribacteres, Tenericutes) between vehicle groups (WT veh and App^{NL-G-F} veh mice). The overall ratio of Firmicutes/Bacteroidetes was decreased in App^{NL-G-F} mice. However, probiotic supplementation of App^{NL-G-F} mice resulted in increased abundance of a few of the bacteria phyla (Verrucomicrobia, Actinobacteria and two unknown phyla) with no change in the overall Firmicutes/Bacteroidetes ratio. Chao richness demonstrated no differences between vehicle and VSL#3 fed WT mice but a significant increase was observed in VSL#3 fed App^{NL-G-F} mice compared to their respective controls (Fig. 1a). Shannon diversity showed a similar lack of differences between VSL#3 and vehicle treated WT mice while VSL#3 fed App^{NL-G-F} mice showed a significant increase in diversity compared to their respective controls (Fig. 1b). In agreement with this, a PCoA plot showed similar clustering for WT vehicle and WT VSL#3 fed mice compared to App^{NL-G-F} mice which demonstrated a very distinct pattern of clustering between vehicle and VSL#3 fed mice (Fig. 1c). These data support the conclusion that VSL#3 feeding significantly altered the enterotype of App^{NL-G-F} mice rather than WT mice.

3.2 App^{NL-G-F} mice had increased intestinal permeability compared to WT control mice

Based upon the observed differences in fecal microbiome and the differences in particularly the App^{NL-G-F} mice fed VSL#3, we anticipated differences in intestinal function. To test the idea that increased leakiness may be a characteristic of disease, an *in vivo* FITC-dextran assay was performed. FITC-conjugated dextran (4 kDa) was administered orally to all the mice and intestinal permeability was assessed by quantifying fluorescence in serum samples. As anticipated, vehicle treated App^{NL-G-F} mice demonstrated clear intestinal dysfunction with significantly increased intestinal permeability compared to vehicle treated WT mice (Fig. 2a). However, supplementation with VSL #3 attenuated the aberrant intestinal permeability of the App^{NL-G-F} mice demonstrating a beneficial effect of probiotic feeding on maintaining intestinal integrity. To examine gastrointestinal motility as another general assessment of function, gastric emptying and the intestinal geometric center were determined in the mice by assessing the distribution of a 70 kDa FITC conjugated dextran throughout the gastrointestinal tract after oral gavage. No changes in either gastric emptying or the intestinal geometric center were observed among the different groups with and without VSL#3 supplementation (Fig. 2 b, c). This demonstrated that the intestinal dysfunction was more specific to barrier function rather than motility.

Author Manuscript Author Manuscript Author Manuscript Author Manuscript

3.3 Intestinal inflammation was increased in App^{NL-G-F} compared to WT mice

Based upon the altered microbiome and apparently compromised barrier function, we hypothesized that *App*$^{NL-G-F}$ mice would demonstrate an inflammatory phenotype in their intestines. To quantify a change in immune phenotype, protein levels of pro-inflammatory cytokines interleukin-1β (IL-1β), interleukin-6 (IL-6), tumor necrosis factor α (TNF-α) and lipocalin were examined by enzyme-linked immunosorbent assay (ELISA) in C57BL/6 (WT) and *App*$^{NL-G-F}$ mice ileums. As predicted, levels of IL-1β and IL-6 were significantly elevated in vehicle treated *App*$^{NL-G-F}$ mice (Fig. 3a, b) with no change in TNF-α levels when compared to WT vehicle mice (Fig. 3c). However, the levels of IL-1β and TNF-α were reduced following VSL#3 supplementation in *App*$^{NL-G-F}$ and WT, respectively. Lipocalin (LCN-2), considered a robust marker of intestinal inflammation (Agostini et al., 2014), was also measured in ileums of WT and *App*$^{NL-G-F}$ mice. Vehicle-treated *App*$^{NL-G-F}$ mice had significantly higher LCN-2 levels when compared to WT vehicle mice (Fig. 3d). Probiotic supplementation of *App*$^{NL-G-F}$ mice decreased LCN-2 levels near to control values. These results validated that *App*$^{NL-G-F}$ mice had a significantly elevated proinflammatory environment in their small intestines as a function of disease that was amenable to repair with VSL#3 feeding. ELISA was performed to assess the levels of Aβ in the ileum. We did not observe any detectable Aβ 1-40 or 1-42 in *App*$^{NL-G-F}$ mice regardless of treatment (Supplemental Fig. 1). This is consistent with our prior study which only detected colon Aβ in younger 3-month-old mice (Manocha et al., 2019).

3.4 Probiotic supplementation decreased inflammatory and increased tight junction proteins in ileums of WT control animals

In order to further quantify the intestinal dysfunction of the *App*$^{NL-G-F}$ mice and any reparative ability of VSL#3 feeding, western blot analyses were performed. The levels of various proteins including beta-secretase 1 (BACE 1), amyloid precursor protein, glial fibrillar acidic protein (GFAP), CD68, cyclooxygenase-2 (COX-2), synapsin I, postsynaptic density protein 95 (PSD-95), inducible nitric oxide synthase (iNOS), cFos, and the tight junction protein, occludin, were quantified from ileal lysates of C57BL/6 (WT) and *App*$^{NL-G-F}$ mice. Somewhat surprisingly, protein levels of BACE1 and GFAP were decreased in vehicle-fed *App*$^{NL-G-F}$ mice when compared to vehicle C57BL/6 (WT) mice (Fig. 4). COX-2 protein levels were also lower in vehicle treated *App*$^{NL-G-F}$ compared to vehicle C57BL/6 (WT) mice (Fig. 4). VSL#3 supplementation had no effect on levels of any of the examined proteins in *App*$^{NL-G-F}$ mice (Fig. 4). On the other hand, VSL#3 feeding had a dramatic effect on WT mice. Probiotic feeding significantly reduced CD68 and iNOS protein levels in the WT mice (Fig. 4). Moreover, levels of the tight junction protein, occludin, were significantly increased in WT mice supplemented with VSL#3 (Fig. 4). This supported results from the permeability assay and the cytokine ELISAs indicating that effects of the probiotic differed between genotypes.

3.5 Serum eicosanoids were elevated in App^{NL-G-F} compared to WT mice and attenuated with VSL#3 feeding

As one means of assessing the peripheral inflammatory state of disease, we examined whether blood levels of eicosanoids were elevated in the *App*$^{NL-G-F}$ mice and altered by

Author Manuscript Author Manuscript Author Manuscript Author Manuscript

probiotic feeding. The levels of serum eicosanoids prostaglandin D (PGD_2), prostaglandin E2 (PGE_2), 6-keto-prostaglandin F1α (6-keto $PGF_{1\alpha}$), prostaglandin F2α ($PGF_{2\alpha}$), and thromboxane B2 (TXB2) along with arachidonic acid and docosahexaenoic acid were estimated using mass spectrometry. Increased levels of PGE2, 6-keto $PGF_{1\alpha}$, $PGF_{2\alpha}$, and TXB2 were observed in vehicle treated $App^{NL\text{-}G\text{-}F}$ mice compared to WT controls (Fig. 5). However, no significant difference was observed in either arachidonic acid or docosahexaenoic acid levels between WT and $App^{NL\text{-}G\text{-}F}$ mice. Interestingly, VSL#3 supplementation of $App^{NL\text{-}G\text{-}F}$ animals significantly decreased serum eicosanoid levels of PGE2, 6-keto $PGF_{1\alpha}$, and $PGF_{2\alpha}$ when compared to the vehicle treated $App^{NL\text{-}G\text{-}F}$ group demonstrating a clear anti-inflammatory effect of the diet. These results demonstrated eicosanoid differences in the pathophysiology of AD and a beneficial effect of probiotic supplementation in reducing these inflammatory markers.

3.6 $App^{NL\text{-}G\text{-}F}$ mice had a distinct serum bile acid profile compared to WT controls

Since serum prostaglandin changes were indicative of a disease phenotype, we next asked whether other serum markers of lipid metabolism could also indicate disease. In particular, in order to better compare to the changes in intestinal microbiota we quantified primary and secondary bile acid levels. Both conjugated and unconjugated primary and secondary bile acids were assessed using mass spectrometry. The primary bile acids α-muricholic acid, β-muricholic acid, ω-muricholic acid, cholic acid (CA) and chenodeoxycholic acid (CDCA) were significantly reduced in serum samples of $App^{NL\text{-}G\text{-}F}$ mice when compared to WT controls (Fig. 6). However, muricholic acid levels conjugated with taurine (tauro-α + ω -muricholic acid, tauro-β-muricholic acid) were significantly elevated in vehicle treated $App^{NL\text{-}G\text{-}F}$ compared to WT mice (Fig. 6). Taurine conjugated deoxycholic acid, chenodeoxycholic acid, taurodeoxycholic, and tauro-chenodeoxycholic were also increased in $App^{NL\text{-}G\text{-}F}$ compared to WT mice (Fig. 6). Secondary bile acids, deoxycholic and lithocholic acid, were significantly reduced in $App^{NL\text{-}G\text{-}F}$ vehicle treated compared to WT mice (Fig. 6).

VSL#3 supplementation of $App^{NL\text{-}G\text{-}F}$ animals altered only taurodeoxycholic acid levels by decreasing concentrations compared to $App^{NL\text{-}G\text{-}F}$ vehicle treated mice. On the other hand, a significant decrease in unconjugated primary and secondary bile acids were observed in VSL#3 supplemented WT mice when compared to their vehicle treated controls. Levels of α-muricholic acid, β-muricholic acid, ω-muricholic acid, CA, chenodeoxycholic acid, deoxycholic acid, lithocholic acid, glycocholic acid (GCA), and ursodeoxycholic acid were all attenuated in WT mice supplemented with VSL#3 compared to their respective controls (Fig. 6). These data verified that specific serum levels of both primary and secondary bile acids were unique to the AD mice, much like the prostaglandins, verifying a dysfunction of lipid metabolism in these animals. However, although WT mice responded robustly to VSL#3 supplementation with attenuated bile acid levels, the $App^{NL\text{-}G\text{-}F}$ bile acid levels were largely resistant to the effect of the probiotic diet.

Author Manuscript Author Manuscript Author Manuscript Author Manuscript

3.7 Probiotic supplementation had no effect on Aβ accumulation, cytokines, or gliosis in App^{NL-G-F} mice

Since VSL#3 feeding attenuated intestinal inflammation, improved intestinal leakiness, and attenuated select serum eicosanoids and bile acid levels, we determined whether any communication of benefit was transferred to the brains by quantifying Aβ and gliosis. Specifically, we performed immunohistochemistry for Aβ, GFAP, and Iba-1. As expected, the results showed increased Aβ deposition in App^{NL-G-F} mice when compared to control animals (Fig. 7). Astrogliosis and microgliosis were also increased significantly in App^{NL-G-F} brains correlating with the increased Aβ deposition. However, VSL#3 supplementation had no significant ability to attenuate either gliosis or Aβ plaque load (Fig. 7).

In order to provide a more quantifiable assessment of brain Aβ levels, ELISAs were next performed. The levels of Aβ 1-40 and Aβ 1-42, both soluble and insoluble, were assessed from the temporal cortices of WT and App^{NL-G-F} mice (Fig. 8). As expected, App^{NL-G-F} mice had significantly elevated levels of soluble and insoluble Aβ 1-40 and 1-42 (Fig. 8). However, probiotic supplementation to App^{NL-G-F} animals had no effect on Aβ levels in brain. To further quantify gliosis-associated changes, western blots were performed to quantify GFAP and Iba-1 levels long with various other protein levels in the temporal cortex of App^{NL-G-F} mice. BACE 1, amyloid precursor protein, GFAP, Iba-1, COX-2, synaptophysin, PSD-95, iNOS, cFos and occludin were examined. The levels of GFAP and Iba-1 along with the neuronal activity marker, cFos, and PSD-95 were all increased in App^{NL-G-F} compared to WT mice (Fig. 9). However, consistent with the lack of effect observed via immunohistochemistry, VSL#3 supplementation did not alter levels of any of the proteins examined.

As a final assessment of overall inflammatory state, levels of several cytokines and LCN-2 were quantified from the brains. Concentrations of IL-1β, IL-6, TNF-α, and LCN-2 were determined by ELISA in WT and App^{NL-G-F} mice. Increased TNF-α is known as a key element in inflammatory cascades and was increased in App^{NL-G-F} compared to WT mice (Fig. 10). Lipocalin was also elevated in App^{NL-G-F} mice compared to controls. The lack of differences between WT and App^{NL-G-F} IL-6 levels may be due to reduced brain ELISA sensitivity, actually no significant differences, or a reciprocal relationship with TNFα (Yimin and Kohanawa, 2006). However, probiotic supplementation had no effect on any of the pro-inflammatory cytokines or LCN-2 levels in the brain.

3.8 App^{NL-G-F} mice had a unique brain eicosanoid profile compared to WT mice

For consistency, we quantified levels of brain eicosanoids PGD_2, PGE_2, 6-keto $PGF_{1\alpha}$, $PGF_{2\alpha}$, and TXB2 along with arachidonic acid and docosahexaenoic acid using mass spectrometry. A decrease in levels of PGD_2, 6-keto $PGF_{1\alpha}$, and $PGF_{2\alpha}$ were observed in vehicle treated App^{NL-G-F} mice to WT vehicle controls, which is the opposite of what was observed in the serum samples (Fig. 11). On the other hand, brain TXB2 and docosahexaenoic acid levels were increased in the vehicle-treated App^{NL-G-F} compared to wild type mice (Fig. 11). This confirmed a disease-associated brain difference of these bioactive lipid metabolites. More importantly, there was one consistency of elevated TXB2

Author Manuscript Author Manuscript Author Manuscript Author Manuscript

levels in both serum and brains of *App*$^{NL-G-F}$ mice. VSL#3 supplementation increased arachidonic acid levels in the *App*$^{NL-G-F}$ mouse brains with no effect on eicosanoid levels. However, VSL#3 feeding significantly decreased PGD_2, PGE_2, 6-keto $PGF_{1\alpha}$, and $PGF_{2\alpha}$ in WT mice demonstrating a genotype selective, potent effect on arachidonic acid metabolism (Fig. 11).

3.9 App^{NL-G-F} mice had a distinct brain bile acid profile compared to WT mice

Since a dramatic serum profile difference in bile acids existed between *App*$^{NL-G-F}$ and WT mice, we assessed whether similar concentration differences existed in the brain. Both conjugated and unconjugated primary and secondary bile acids were quantified from the temporal cortex of the mice using mass spectrometry (Fig. 12). ω-muricholic acid levels were significantly lower in vehicle treated *App*$^{NL-G-F}$ compared to WT mice, with no differences in α or β-muricholic acid levels. Taurocholic acid, taurodeoxycholic, tauro α+ ω muricholic acid, and tauro-β muricholic acid levels were also decreased in *App*$^{NL-G-F}$ compared to WT mice which is opposite of what we observed in serum. CA and deoxycholic acid levels were also significantly lower in *App*$^{NL-G-F}$ vehicle-treated mice when compared to controls (Fig. 12). Despite the differences in concentrations across brain and serum analysis, there were consistently lower levels of ω-muricholic acid, CA, and deoxycholic acid in both serum and brains of *App*$^{NL-G-F}$ compared to WT mice. VSL#3 supplementation of *App*$^{NL-G-F}$ animals resulted in no difference in any of the bile acids when compared to vehicle *App*$^{NL-G-F}$ mice unlike the reduction in taurodeoxycholic acid observed in serum (Fig. 12). On the other hand, significant decreases in all taurine-conjugated bile acid levels, taurocholic acid, taurodeoxycholic, tauro α+ ω muricholic acid, and tauro-β muricholic acid were observed in VSL#3 supplemented WT mice (Fig. 12). This is consistent with the observed serum changes in bile acid levels in which WT mice were more responsive to VSL#3 feeding compared to *App*$^{NL-G-F}$ mice. Lithocholic acids and glycochenodeoxycholic acid (GCDCA) were not detected in the temporal cortex.

3.10. Probiotic supplementation had no effect on memory function in App^{NL-G-F} mice

Since memory problems are one of the first signs of cognitive impairment related to AD, we tested the mice for working memory using a cross-maze rodent behavior test. As expected, vehicle-treated *App*$^{NL-G-F}$ mice had reduced alternations compared to vehicle-treated WT mice suggesting an impairment in memory function (Fig. 13). However, VSL#3 supplementation had no significant effect on memory performance in either the *App*$^{NL-G-F}$ or WT mice.

4.0 Discussion

We have demonstrated a largely undescribed component of pathophysiology manifesting in the intestines of the *App*$^{NL-G-F}$ mouse model of AD and addressed it using a dietary intervention of probiotic medical food. Although AD is not classically associated with intestinal dysfunction, there are several reports indicating this may be the case. For example, constipation is common among elderly dementia patients (Bassotti et al., 2007; Sandman et al., 1983). Volvulus, constipation, and megacolon have also been significantly associated with AD (Sonnenberg et al., 1994). We and others have shown Aβ and phospho-tau

Author Manuscript Author Manuscript Author Manuscript Author Manuscript

immunoreactivity in AD intestines (Dugger et al., 2016; Joachim et al., 1989; Puig et al., 2015). This study provides compelling evidence, using the $App^{NL\text{-}G\text{-}F}$ mouse model of AD, that a component of the disease pathophysiology is characterized not only by a distinct intestinal dysbiosis and serum/brain bile acid and eicosanoid profiles but also increased intestinal inflammation and permeability. Supplementation of animals with probiotic, VSL#3, for eight weeks altered the gut microbiota and produced a significant decrease in intestinal permeability, serum eicosanoids levels, and intestinal inflammation. These data provide validation of a new therapeutic strategy of using probiotics for the treatment of the AD-associated intestinal pathophysiology. However, our findings also demonstrate that mechanisms regulating communication of intestinal changes to the brain require further elucidation as our ability to demonstrate brain changes was limited. We are cautious in our overall interpretation of results as the WT and $App^{NL\text{-}G\text{-}F}$ mice were not littermate controls and additional characterization of the plethora of VSL#3-mediated brain effects is needed. However, since there were numerous treatment differences within both the wild type and the $App^{NL\text{-}G\text{-}F}$ lines, independently, the findings have relevance to probiotic feeding effects, in particular.

Fecal dysbiosis was a significant aspect of the intestinal manifestation of disease we observed in in the $App^{NL\text{-}G\text{-}F}$ mouse model of AD. We identified a change in the ratio of Firmicutes/Bacteroidetes, comparing WT to $App^{NL\text{-}G\text{-}F}$ mice. Interestingly, changes in this ratio are also observed in various metabolic disorders and conditions including obesity and aging in both humans and rodents (Ley et al., 2006; Mariat et al., 2009). Prior studies primarily relying upon the APP/PS1 or 3xTg mouse lines have also documented a distinct disease enterotype that differs with age and correlates with cognitive dysfunction (Bauerl et al., 2018; Brandscheid et al., 2017; Park et al., 2017; Shen et al., 2017; Zhang et al., 2017). Discrepancies in the abundance of phyla previously reported in APP/PS1 line versus our findings in the $App^{NL\text{-}G\text{-}F}$ mice may be due to differences in mutant APP expression, mouse ages, or even housing and diet differences. Others have shown that extended oral antibacterial treatment can lead to decreased plaque load and altered gliosis in the APP/PS1 line supporting the idea that intestinal bacteria actively contribute to disease (Minter et al., 2016). Perhaps our limited brain effects are due to a lower treatment time, dosage, or the particular choice of probiotic we used. We fully appreciate that there are species differences in intestinal microbiota when comparing mice to humans. For example, the high abundance of Lactobacillus and scarcity of Faecelibacterium in murine intestines have exactly the opposite ratio in humans (Hugenholtz and de Vos, 2018). Nevertheless, we observed a very similar decrease in Firmicutes and increase in Bacteroidetes in the fecal samples of $App^{NL\text{-}G\text{-}F}$ mice as has been reported from the intestinal microbiome of AD subjects compared to age- and sex-matched individuals (Vogt et al., 2017). These phyla are heavily involved in metabolism of undigested food as well as digestion of dietary fibers and polyphenols by a complex energy harvesting mechanism generating short chain fatty acids butyrate, acetate, and propionate (SCFAs) (Macfarlane and Macfarlane, 2003). Altered abundance of these phyla may indeed affect the intestinal permeability and inflammatory changes we observed in $App^{NL\text{-}G\text{-}F}$ mice.

Our approach to attenuating these intestinal aspects of disease relied upon administering the medical food, VSL#3, to alter the microbiota. Although the mechanisms underlying the

Author Manuscript Author Manuscript Author Manuscript Author Manuscript

therapeutic effects of VSL#3 are not completely known, it has been suggested that VSL#3 elicits its effects through changing gut microbiota composition, inhibition of bacterial translocation, modulation of immune cell responses, enhanced expression of tight junction proteins, increased production of cell surface mucin, reduced adhesion of pathogens to the intestinal mucosa, increased production of antimicrobial compounds, increased epithelial cell survival, and production of bacteria-derived metabolites including SCFAs (Abalan et al., 1990; Dai et al., 2012; Madsen et al., 2001; Pagnini et al., 2010; Uronis et al., 2011; Wang et al., 2018; Yadav et al., 2013). Based upon these previous observations, we hypothesized that VSL#3 supplementation would attenuate the intestinal aspects of disease. Supplementing the AD mice with probiotic for eight weeks resulted in increased abundance of Verrucomicrobia and Actinobacteria, supporting the ability of VSL#3 to alter the gut bacterial composition in the $App^{NL\text{-}G\text{-}F}$ mice. Actinobacteria represent one of the largest bacterial phyla and are Gram-positive filamentous bacteria with a high G+C content in their genomes. Metagenomic studies from human fecal samples have revealed Actinobacteria as one of the six dominant phyla (Eckburg et al., 2005). Within this phylum, higher numbers of Bifidobacterium are associated with reduced intestinal inflammation and improved epithelial barrier integrity (Krumbeck et al., 2018; Mendes et al., 2018; Paveljsek et al., 2018). *Akkermansia muciniphila* of the Verrucomicrobia phylum is known to metabolizes mucin to produce small chain fatty acids, propionate and acetate, in particular (Ottman et al., 2017). High levels of *A. muciniphilia* are also generally associated with a healthy intestinal tract with lower levels correlating with obesity, diabetes, appendicitis, and inflammatory bowel disease (Dao et al., 2016; Karlsson et al., 2012; Plovier et al., 2017; Png et al., 2010; Rajilic-Stojanovic et al., 2013; Swidsinski et al., 2011; Zhang et al., 2013). Even though these phyla changes from VL#3 feeding were robust, it was surprising that the fecal microbiome changes were not reflective of the species in VSL#3. Although VSL#3 has been demonstrated to be relatively viable up to 2 hours in simulated gastric and intestinal fluid (Vecchione et al., 2018), it is possible that the bacteria did not survive long enough to colonize the intestines. Alternatively, high amount of host DNA or limited sequencing depth likely limited our ability to identify low abundance species (Pereira-Marques et al., 2019). It is not entirely expected, however, that probiotics will be able to replicate sufficiently to colonize and displace the resident rodent commensal bacteria. In fact, the probiotics may serve simply as transient stimuli, of either living or dead bacteria, to both the resident intestinal microbiome as well as the host intestinal cells to exert their influence (Zmora et al., 2018). In addition, our analysis of fecal microbiome may not accurately reflect bacteria that were effective in adhering to the mucosa to colonize and future comparison will require assessment of mucosal and fecal microbiome during disease and intervention.

Unlike our study focused on intestinal components of disease, several groups have published efforts to manipulate the intestinal microbiota in AD mice to affect the brain through the so-called gut-brain axis. There are several mechanisms proposed by which probiotic can modulate brain functions including vagal signaling (Bravo et al., 2011), neuronal pathways (Baik et al., 2014), microbial metabolites such as short chain fatty acid including acetate, butyrate, and lactate (Macfabe, 2012; Macfarlane and Macfarlane, 2003; Moretti et al., 2011), and bacterial-immune interaction (Donato et al., 2010; Zareie et al., 2006). It is unclear why we did not observe robust brain effects on Aβ plaque load, gliosis or cytokine

Author Manuscript Author Manuscript Author Manuscript Author Manuscript

changes in our probiotic fed mice. It could be possible that our feeding paradigm or the particular probiotic choice may have minimized our ability to observe any brain effects. In addition, our use of females only may explain the lack of changes in gliosis and cytokines following probiotic supplementation. Sex differences in the clinical phenotype and progression of AD have been well documented (Cavedo et al., 2018). In fact, recent studies have shown sex-specific effects of microbiome perturbations on cerebral Aβ amyloidosis and microglia phenotypes. Male but not female APP/PS1 mice demonstrated a significant reduction of Aβ deposition along with microglial morphological alterations following antibiotic treatment (Dodiya et al., 2019). Others have reported robust observation in the brain from longer interventions. For example, feeding a probiotic containing *Bifidobacterium longum* and *Lactobacillus acidophilus* to male APP/PS1 mice starting at 3 months for 20 weeks resulted in decreased plaque area without affecting microglia numbers (Abraham et al., 2019). 12-weeks of combined treatment of *L. plantarum* with memantine ameliorated cognitive deterioration, decreased Aβ levels in the hippocampus, and protected neuronal integrity and plasticity (Wang et al., 2020). Feeding 3xTg-AD mice a probiotic mixture at eight weeks for an additional 16 weeks resulted in decreased markers of oxidative stress (Bonfili et al., 2018). A similar study feeding 3xTg-AD mice the same probiotic mixture demonstrated that it was sufficient to attenuate levels of Aβ, plasma cytokines, and cell death in the AD mice (Bonfili et al., 2017). Collectively, these findings support the idea that manipulating the intestinal microbiota in rodents can improve intestinal aspects of disease, as we have demonstrated, but also exert benefits in the brain given a particular treatment paradigm.

Prostaglandins are one of the possible molecules communicating a gut-brain response. For example, a disrupted intestinal barrier results in translocation of luminal contents including microbes and their products into the systemic circulation which certainly have detrimental consequences, including activation of the peripheral immune system (Brenchley and Douek, 2012). Prostaglandins are inflammatory lipid mediators that can be released from immune cells to cross the blood brain barrier and are important communication molecules connecting the brain and the systemic immune system. We observed a significant increase in serum levels of PGE2, 6-keto $PGF_{1\alpha}$, $PGF_{2\alpha}$, and TXB_2 in $App^{NL\text{-}G\text{-}F}$ mice supporting the existence of systemic inflammation. Moreover, this increase in lipid mediators was attenuated by probiotic feeding correlating with the observed decrease in proinflammatory cytokines noted in the intestines. These results are consistent with a previous study that showed a significant decrease in eicosanoids levels and colitis following VSL#3 treatment in a rat model of experimental colitis (Shibolet et al., 2002). Interestingly, only TXB2 was elevated in the brains of $App^{NL\text{-}G\text{-}F}$ mice but was not attenuated by VSL#3 feeding. Previous studies have demonstrated that activated microglial robustly secrete TXB2 in the CNS (Giulian et al., 1996). Therefore, increased microglial production of TXB2 in the brains of the $App^{NL\text{-}G\text{-}F}$ mice could have masked any probiotic-dependent attenuation of blood-derived TXB2 in the brain. It appears that, although elevated TXB2 was a consistent blood and brain biomarker of disease, intestinal microbiota changes only influenced the increase in the serum. Additional optimization of the feeding paradigm may better address whether the brain elevation of TXB2 can be attenuated with dietary probiotic intervention.

Author Manuscript Author Manuscript Author Manuscript Author Manuscript

Another possible communicating molecule from the intestine to the brain could be bile acids. Bile acids are capable of influencing neurotransmission, neuroendocrine responses, physiology, and neurogenesis indicating an important role for these signaling mediators in brain homeostasis (McMillin and DeMorrow, 2016). Interestingly, a dramatic difference in bile acid concentrations in the serum of *App*$^{NL-G-F}$ mice was observed, particularly a decrease in secondary bile acids, unconjugated primary bile acids and increase in most of the conjugated primary bile acids was found when compared to WT mice. Gut microbiota composition can modify the bile acid profile through a broad range of reactions including conjugation and deconjugation resulting in formation of secondary bile acids (Duboc et al., 2013; Jones et al., 2014; Musso et al., 2011; Ridlon et al., 2014; Theriot et al., 2014). Interestingly, alteration in the bile acid profile has been associated with cognitive impairment in AD (Andy et al., 2016; Bauer et al., 1991). Our mass spectrometric analysis of serum showed a significant increase in taurine conjugated muricholic acid (tauro-α-muricholic acid, tauro-β-muricholic acid) in vehicle treated *App*$^{NL-G-F}$ mice when compared to controls. Taurine conjugated deoxycholic acid (taurodeoxycholic), chenodeoxycholic acid (tauro-chenodeoxycholic) and ursodeoxycholic acid were also increased in *App*$^{NL-G-F}$ mice. Increased conjugated bile acids in the serum suggests decreased bile salt hydrolase (BSH) enzyme-producing bacteria in the intestine including *Lactobacillus, Bifidobacterium, Clostridium, andBacteroides sps.* (Begley et al., 2006).

Surprisingly, many of the bile acids (primary and secondary) were significantly reduced in *App*$^{NL-G-F}$ brains compared to controls consistent with a study performed using APP/PS1 mice showing decreased levels of CA, ω-muricholic acid, TCA, and tauro-α and β-muricholic acids compared to wild type controls (Pan et al., 2017). This suggests a complex regulation in which the levels of bile acids in the serum are regulated independently from brain. Nevertheless, since bile acid production can be modulated by metabolic activity of the gut microbiota, it is likely that the dysbiosis observed in the *App*$^{NL-G-F}$ intestines are related to the altered bile acid profiles in the brains. For example, although tauroursodeoxycholic acid (TUDCA) was elevated in the serum of *App*$^{NL-G-F}$ mice, TUDCA levels were drastically decreased in *App*$^{NL-G-F}$ mouse brains compared to controls. TUDCA is a neuroprotective bile conjugate and has been studied in several animal models of neurodegenerative disease, including Huntington's and Parkinson's disease as well as brain injury (Keene et al., 2002; Keene et al., 2001; Sun et al., 2017). Recently, the therapeutic efficacy of exogenously provided TUDCA has also been reported in APP/PS1 mice (Dionisio et al., 2015; Nunes et al., 2012). However, VSL#3 feeding provided no change in brain levels of TUDCA in App^{NL-G-F} mice and actually decreased levels in WT mice. In fact, probiotic treatment increased brain concentrations of β-muricholic acid with a decrease in taurine conjugated muricholic acid, deoxycholic and ursodeoxycholic acid in only WT mice suggesting VSL#3 decreased bile acid taurine conjugation in a genotype selective fashion. Only DCA was found to be decreased in both brain and serum samples of App^{NL-G-F} compared to WT mice. These results are supported by previous studies suggesting that bile acids may be synthesized locally in the brain directly from cholesterol and are not from hepatic origin (Mano et al., 2004; Quinn, 2013). Therefore, further studies are required to investigate if bile acids in the brain are unique to the disease phenotype and

Author Manuscript Author Manuscript Author Manuscript Author Manuscript

determine whether manipulation of their concentrations could be targeted as a therapeutic strategy.

We observed that VSL#3 feeding for eight weeks had no significant effect on memory improvement. This lack of change could be related to the particular probiotic or the paradigm we employed. For example, our use of probiotics at an advanced stage of amyloidosis/gliosis may not be ideal. Some recent literature suggests that probiotic treatment alone is not effective in improving spatial memory in AD mice requiring, for example, a combined treatment of exercise and probiotic to increase brain performance (Abraham et al., 2019). Future studies are required to test probiotic interventions singly or in combination in a variety of models and paradigms to best assess the potential of this therapeutic strategy.

In summary, our study provides evidence of an intestinal manifestation of disease using the *App*$^{NL-G-F}$ mouse model. The pathology included increased permeability and inflammatory state and correlated with elevated levels of select prostaglandins and bile acids in the serum. Probiotic supplementation exerted a beneficial effect by reducing intestinal inflammation and permeability in correlation with altered levels of select serum prostaglandins and bile acids in both wild type and *App*$^{NL-G-F}$ mice. In addition, VSL#3 feeding had a significant effect on select prostaglandins and bile acids in the brains of wild type mice demonstrating a novel effect of this dietary supplementation. However, brain changes associated with AD, including increased cytokine levels, Aβ plaque load, and gliosis, were resistant to the particular probiotic intervention paradigm we employed. Further study will better define the intestinal dysfunction of AD in both mouse models and humans to determine whether it influences brain changes. Dietary manipulation through probiotic intervention appears to be an attractive means of attenuating the intestinal aspect of disease.

Supplementary Material

Refer to Web version on PubMed Central for supplementary material.

Acknowledgements

This work was supported by funding from Alzheimer's Association Research fellowship, AARF-17-533143, a University of North Dakota (UND) Post-Doc Pilot Grant, the North Dakota Experimental Program to Stimulate Competitive Research (ND EPSCoR), UND0021228, and National Institutes of Health 5R01AG048993, 5P20GM113123, U54GM128729, and P20GM103442. We thank Drs. Takashi Saito and Takaomi Saido, Laboratory for Proteolytic Neuroscience, RIKEN Center for Brain Science, Wako-shi, Saitama, Japan for kindly providing *App*$^{NL-G-F}$ mice. The authors also thank Angela M Floden, Dr. Gunjan D Manocha, Dr. Joshua A. Kulas, and Mona Sohrabi, for their help in animal/tissue collection.

Harpreet Kaur: Funding Acquisition, Conceptualization, Methodology, Formal Analysis, Writing-Original Draft, Writing-Review & Editing, Visualization **Kumi Nagamoto-Combs:** Investigation, Writing-Review & Editing **Svetlana Golovko**: Investigation, Methodology **Mikhail Y Golovko**, Investigation, Methodology, Visualization **Marilyn G Klug**: Formal Analysis, Visualization **Colin Combs**: Funding Acquisition, Conceptualization, Supervision, Project Administration, Writing-Review & Editing, Visualization

Author Manuscript Author Manuscript Author Manuscript Author Manuscript

References

Abalan F, Jouan A, Weerts MT, Solles C, Brus J, Sauneron MF, 1990 A study of digestive absorption in four cases of Down's syndrome. Down's syndrome, malnutrition, malabsorption, and Alzheimer's disease. Med Hypotheses 31(1), 35–38. [PubMed: 2138242]

Abraham D, Feher J, Scuderi GL, Szabo D, Dobolyi A, Cservenak M, Juhasz J, Ligeti B, Pongor S, Gomez-Cabrera MC, Vina J, Higuchi M, Suzuki K, Boldogh I, Radak Z, 2019 Exercise and probiotics attenuate the development of Alzheimer's disease in transgenic mice: Role of microbiome. Exp Gerontol 115, 122–131. [PubMed: 30529024]

Aderem A, Underhill DM, 1999 Mechanisms of phagocytosis in macrophages. Annu Rev Immunol 17, 593–623. [PubMed: 10358769]

Adriani A, Fagoonee S, De Angelis C, Altruda F, Pellicano R, 2014 Helicobacter pylori infection and dementia: can actual data reinforce the hypothesis of a causal association? Panminerva Med 56(3), 195–199. [PubMed: 25056243]

Agostini S, Clerici M, Mancuso R, 2014 How plausible is a link between HSV-1 infection and Alzheimer's disease? Expert Rev Anti Infect Ther 12(3), 275–278. [PubMed: 24502805]

Akbari E, Asemi Z, Daneshvar Kakhaki R, Bahmani F, Kouchaki E, Tamtaji OR, Hamidi GA, Salami M, 2016 Effect of Probiotic Supplementation on Cognitive Function and Metabolic Status in Alzheimer's Disease: A Randomized, Double-Blind and Controlled Trial. Frontiers in aging neuroscience 8, 256. [PubMed: 27891089]

Andreasson KI, Bachstetter AD, Colonna M, Ginhoux F, Holmes C, Lamb B, Landreth G, Lee DC, Low D, Lynch MA, Monsonego A, O'Banion MK, Pekny M, Puschmann T, Russek-Blum N, Sandusky LA, Selenica ML, Takata K, Teeling J, Town T, Van Eldik LJ, 2016 Targeting innate immunity for neurodegenerative disorders of the central nervous system. J Neurochem 138(5), 653–693. [PubMed: 27248001]

Andy UU, Vaughan CP, Burgio KL, Alli FM, Goode PS, Markland AD, 2016 Shared Risk Factors for Constipation, Fecal Incontinence, and Combined Symptoms in Older U.S. Adults. J Am Geriatr Soc 64(11), e183–e188. [PubMed: 27783401]

Arai H, Lee VM, Messinger ML, Greenberg BD, Lowery DE, Trojanowski JQ, 1991 Expression patterns of beta-amyloid precursor protein (beta-APP) in neural and nonneural human tissues from Alzheimer's disease and control subjects. Ann Neurol 30(5), 686–693. [PubMed: 1763893]

Arendash GW, Gordon MN, Diamond DM, Austin LA, Hatcher JM, Jantzen P, DiCarlo G, Wilcock D, Morgan D, 2001 Behavioral assessment of Alzheimer's transgenic mice following long-term Abeta vaccination: task specificity and correlations between Abeta deposition and spatial memory. DNA Cell Biol 20(11), 737–744. [PubMed: 11788052]

Aube AC, Cabarrocas J, Bauer J, Philippe D, Aubert P, Doulay F, Liblau R, Galmiche JP, Neunlist M, 2006 Changes in enteric neurone phenotype and intestinal functions in a transgenic mouse model of enteric glia disruption. Gut 55(5), 630–637. [PubMed: 16236773]

Austin SA, Combs CK, 2010 Amyloid precursor protein mediates monocyte adhesion in AD tissue and apoE(−)/(−) mice. Neurobiology of aging 31(11), 1854–1866. [PubMed: 19058878]

Baik SH, Cha MY, Hyun YM, Cho H, Hamza B, Kim DK, Han SH, Choi H, Kim KH, Moon M, Lee J, Kim M, Irimia D, Mook-Jung I, 2014 Migration of neutrophils targeting amyloid plaques in Alzheimer's disease mouse model. Neurobiology of aging 35(6), 1286–1292. [PubMed: 24485508]

Balin BJ, Little CS, Hammond CJ, Appelt DM, Whittum-Hudson JA, Gerard HC, Hudson AP, 2008 Chlamydophila pneumoniae and the etiology of late-onset Alzheimer's disease. Journal of Alzheimer's disease : JAD 13(4), 371–380. [PubMed: 18487846]

Bassotti G, Villanacci V, Fisogni S, Cadei M, Di Fabio F, Salerni B, 2007 Apoptotic phenomena are not a major cause of enteric neuronal loss in constipated patients with dementia. Neuropathology 27(1), 67–72. [PubMed: 17319285]

Bauer J, Konig G, Strauss S, Jonas U, Ganter U, Weidemann A, Monning U, Masters CL, Volk B, Berger M, et al., 1991 In-vitro matured human macrophages express Alzheimer's beta A4-amyloid precursor protein indicating synthesis in microglial cells. FEBS Lett 282(2), 335–340. [PubMed: 1903718]

Author Manuscript Author Manuscript Author Manuscript Author Manuscript

Bauerl C, Collado MC, Diaz Cuevas A, Vina J, Perez Martinez G, 2018 Shifts in gut microbiota composition in an APP/PSS1 transgenic mouse model of Alzheimer's disease during lifespan. Lett Appl Microbiol 66(6), 464–471. [PubMed: 29575030]

Begley M, Hill C, Gahan CG, 2006 Bile salt hydrolase activity in probiotics. Appl Environ Microbiol 72(3), 1729–1738. [PubMed: 16517616]

Bonfili L, Cecarini V, Berardi S, Scarpona S, Suchodolski JS, Nasuti C, Fiorini D, Boarelli MC, Rossi G, Eleuteri AM, 2017 Microbiota modulation counteracts Alzheimer's disease progression influencing neuronal proteolysis and gut hormones plasma levels. Scientific reports 7(1), 2426. [PubMed: 28546539]

Bonfili L, Cecarini V, Cuccioloni M, Angeletti M, Berardi S, Scarpona S, Rossi G, Eleuteri AM, 2018 SLAB51 Probiotic Formulation Activates SIRT1 Pathway Promoting Antioxidant and Neuroprotective Effects in an AD Mouse Model. Mol Neurobiol 55(10), 7987–8000. [PubMed: 29492848]

Brandscheid C, Schuck F, Reinhardt S, Schafer KH, Pietrzik CU, Grimm M, Hartmann T, Schwiertz A, Endres K, 2017 Altered Gut Microbiome Composition and Tryptic Activity of the 5xFAD Alzheimer's Mouse Model. Journal of Alzheimer's disease : JAD 56(2), 775–788. [PubMed: 28035935]

Bravo JA, Forsythe P, Chew MV, Escaravage E, Savignac HM, Dinan TG, Bienenstock J, Cryan JF, 2011 Ingestion of Lactobacillus strain regulates emotional behavior and central GABA receptor expression in a mouse via the vagus nerve. Proc Natl Acad Sci U S A 108(38), 16050–16055. [PubMed: 21876150]

Brenchley JM, Douek DC, 2012 Microbial translocation across the GI tract. Annu Rev Immunol 30, 149–173. [PubMed: 22224779]

Brito MV, Yasojima EY, Teixeira RK, Houat Ade P, Yamaki VN, Costa FL, 2015 Fasting does not induce gastric emptying in rats. Acta cirurgica brasileira 30(3), 165–169. [PubMed: 25790003]

Brose S, Baker A, Golovko M, 2013 A Fast One-Step Extraction and UPLC-MS/MS Analysis for E2/D2 Series Prostaglandins and Isoprostanes. Lipids 48(4), 411–419. [PubMed: 23400687]

Brose SA, Baker AG, Golovko MY, 2013 A fast one-step extraction and UPLC-MS/MS analysis for E2/D 2 series prostaglandins and isoprostanes. Lipids 48(4), 411–419. [PubMed: 23400687]

Brose SA, Golovko MY, 2012 A rapid oxygen exchange on prostaglandins in plasma represents plasma esterase activity that is inhibited by diethylumbelliferyl phosphate with high affinity. Rapid Commun Mass Spectrom 26(20), 2472–2476. [PubMed: 22976214]

Carding S, Verbeke K, Vipond DT, Corfe BM, Owen LJ, 2015 Dysbiosis of the gut microbiota in disease. Microb Ecol Health Dis 26, 26191. [PubMed: 25651997]

Cavedo E, Chiesa PA, Houot M, Ferretti MT, Grothe MJ, Teipel SJ, Lista S, Habert MO, Potier MC, Dubois B, Hampel H, Group, I.N.-p.S., Alzheimer Precision Medicine, I., 2018 Sex differences in functional and molecular neuroimaging biomarkers of Alzheimer's disease in cognitively normal older adults with subjective memory complaints. Alzheimers Dement 14(9), 1204–1215. [PubMed: 30201102]

Chan YK, El-Nezami H, Chen Y, Kinnunen K, Kirjavainen PV, 2016 Probiotic mixture VSL#3 reduce high fat diet induced vascular inflammation and atherosclerosis in ApoE(−/−) mice. AMB Express 6(1), 61. [PubMed: 27576894]

Chen J, Chia N, Kalari KR, Yao JZ, Novotna M, Paz Soldan MM, Luckey DH, Marietta EV, Jeraldo PR, Chen X, Weinshenker BG, Rodriguez M, Kantarci OH, Nelson H, Murray JA, Mangalam AK, 2016 Multiple sclerosis patients have a distinct gut microbiota compared to healthy controls. Scientific reports 6, 28484. [PubMed: 27346372]

Dai C, Zhao DH, Jiang M, 2012 VSL#3 probiotics regulate the intestinal epithelial barrier in vivo and in vitro via the p38 and ERK signaling pathways. Int J Mol Med 29(2), 202–208. [PubMed: 22089663]

Dao MC, Everard A, Aron-Wisnewsky J, Sokolovska N, Prifti E, Verger EO, Kayser BD, Levenez F, Chilloux J, Hoyles L, Consortium MI-O, Dumas ME, Rizkalla SW, Dore J, Cani PD, Clement K, 2016 Akkermansia muciniphila and improved metabolic health during a dietary intervention in obesity: relationship with gut microbiome richness and ecology. Gut 65(3), 426–436. [PubMed: 26100928]

Author Manuscript Author Manuscript Author Manuscript Author Manuscript

Dhawan G, Combs CK, 2012 Inhibition of Src kinase activity attenuates amyloid associated microgliosis in a murine model of Alzheimer's disease. J Neuroinflammation 9, 117. [PubMed: 22673542]

Dhiman RK, Rana B, Agrawal S, Garg A, Chopra M, Thumburu KK, Khattri A, Malhotra S, Duseja A, Chawla YK, 2014 Probiotic VSL#3 reduces liver disease severity and hospitalization in patients with cirrhosis: a randomized, controlled trial. Gastroenterology 147(6), 1327–1337 e1323. [PubMed: 25450083]

Dinan TG, Stilling RM, Stanton C, Cryan JF, 2015 Collective unconscious: how gut microbes shape human behavior. J Psychiatr Res 63, 1–9. [PubMed: 25772005]

Dionisio PA, Amaral JD, Ribeiro MF, Lo AC, D'Hooge R, Rodrigues CM, 2015 Amyloid-beta pathology is attenuated by tauroursodeoxycholic acid treatment in APP/PS1 mice after disease onset. Neurobiology of aging 36(1), 228–240. [PubMed: 25443293]

Dodiya HB, Kuntz T, Shaik SM, Baufeld C, Leibowitz J, Zhang X, Gottel N, Zhang X, Butovsky O, Gilbert JA, Sisodia SS, 2019 Sex-specific effects of microbiome perturbations on cerebral Abeta amyloidosis and microglia phenotypes. J Exp Med 216(7), 1542–1560. [PubMed: 31097468]

Donato KA, Gareau MG, Wang YJ, Sherman PM, 2010 Lactobacillus rhamnosus GG attenuates interferon-{gamma} and tumour necrosis factor-alpha-induced barrier dysfunction and pro-inflammatory signalling. Microbiology 156(Pt 11), 3288–3297. [PubMed: 20656777]

Duboc H, Rajca S, Rainteau D, Benarous D, Maubert MA, Quervain E, Thomas G, Barbu V, Humbert L, Despras G, Bridonneau C, Dumetz F, Grill JP, Masliah J, Beaugerie L, Cosnes J, Chazouilleres O, Poupon R, Wolf C, Mallet JM, Langella P, Trugnan G, Sokol H, Seksik P, 2013 Connecting dysbiosis, bile-acid dysmetabolism and gut inflammation in inflammatory bowel diseases. Gut 62(4), 531–539. [PubMed: 22993202]

Dugger BN, Whiteside CM, Maarouf CL, Walker DG, Beach TG, Sue LI, Garcia A, Dunckley T, Meechoovet B, Reiman EM, Roher AE, 2016 The Presence of Select Tau Species in Human Peripheral Tissues and Their Relation to Alzheimer's Disease. Journal of Alzheimer's disease : JAD 51(2), 345–356. [PubMed: 26890756]

Eckburg PB, Bik EM, Bernstein CN, Purdom E, Dethlefsen L, Sargent M, Gill SR, Nelson KE, Relman DA, 2005 Diversity of the human intestinal microbial flora. Science 308(5728), 1635–1638. [PubMed: 15831718]

Evrensel A, Ceylan ME, 2015 The Gut-Brain Axis: The Missing Link in Depression. Clin Psychopharmacol Neurosci 13(3), 239–244. [PubMed: 26598580]

Finegold SM, Dowd SE, Gontcharova V, Liu C, Henley KE, Wolcott RD, Youn E, Summanen PH, Granpeesheh D, Dixon D, Liu M, Molitoris DR, Green JA 3rd, 2010 Pyrosequencing study of fecal microflora of autistic and control children. Anaerobe 16(4), 444–453. [PubMed: 20603222]

Gerber GK, 2014 The dynamic microbiome. FEBS Lett 588(22), 4131–4139. [PubMed: 24583074]

Giulian D, Corpuz M, Richmond B, Wendt E, Hall ER, 1996 Activated microglia are the principal glial source of thromboxane in the central nervous system. Neurochem Int 29(1), 65–76. [PubMed: 8808790]

Golovko MY, Murphy EJ, 2008 An improved LC-MS/MS procedure for brain prostanoid analysis using brain fixation with head-focused microwave irradiation and liquid-liquid extraction. J Lipid Res 49(4), 893–902. [PubMed: 18187404]

Guinane CM, Cotter PD, 2013 Role of the gut microbiota in health and chronic gastrointestinal disease: understanding a hidden metabolic organ. Therap Adv Gastroenterol 6(4), 295–308.

Harach T, Marungruang N, Duthilleul N, Cheatham V, Mc Coy KD, Frisoni G, Neher JJ, Fak F, Jucker M, Lasser T, Bolmont T, 2017 Reduction of Abeta amyloid pathology in APPPS1 transgenic mice in the absence of gut microbiota. Scientific reports 7, 41802. [PubMed: 28176819]

Hugenholtz F, de Vos WM, 2018 Mouse models for human intestinal microbiota research: a critical evaluation. Cell Mol Life Sci 75(1), 149–160. [PubMed: 29124307]

Jandhyala SM, Talukdar R, Subramanyam C, Vuyyuru H, Sasikala M, Nageshwar Reddy D, 2015 Role of the normal gut microbiota. World J Gastroenterol 21(29), 8787–8803. [PubMed: 26269668]

Joachim CL, Mori H, Selkoe DJ, 1989 Amyloid beta-protein deposition in tissues other than brain in Alzheimer's disease. Nature 341(6239), 226–230. [PubMed: 2528696]

Author Manuscript Author Manuscript Author Manuscript Author Manuscript

Jones ML, Martoni CJ, Ganopolsky JG, Labbe A, Prakash S, 2014 The human microbiome and bile acid metabolism: dysbiosis, dysmetabolism, disease and intervention. Expert Opin Biol Ther 14(4), 467–482. [PubMed: 24479734]

Karlsson CL, Onnerfalt J, Xu J, Molin G, Ahrne S, Thorngren-Jerneck K, 2012 The microbiota of the gut in preschool children with normal and excessive body weight. Obesity (Silver Spring) 20(11), 2257–2261. [PubMed: 22546742]

Kau AL, Ahern PP, Griffin NW, Goodman AL, Gordon JI, 2011 Human nutrition, the gut microbiome and the immune system. Nature 474(7351), 327–336. [PubMed: 21677749]

Keene CD, Rodrigues CM, Eich T, Chhabra MS, Steer CJ, Low WC, 2002 Tauroursodeoxycholic acid, a bile acid, is neuroprotective in a transgenic animal model of Huntington's disease. Proc Natl Acad Sci U S A 99(16), 10671–10676. [PubMed: 12149470]

Keene CD, Rodrigues CM, Eich T, Linehan-Stieers C, Abt A, Kren BT, Steer CJ, Low WC, 2001 A bile acid protects against motor and cognitive deficits and reduces striatal degeneration in the 3-nitropropionic acid model of Huntington's disease. Exp Neurol 171(2), 351–360. [PubMed: 11573988]

Krumbeck JA, Rasmussen HE, Hutkins RW, Clarke J, Shawron K, Keshavarzian A, Walter J, 2018 Probiotic Bifidobacterium strains and galactooligosaccharides improve intestinal barrier function in obese adults but show no synergism when used together as synbiotics. Microbiome 6(1), 121. [PubMed: 29954454]

Ley RE, Turnbaugh PJ, Klein S, Gordon JI, 2006 Microbial ecology: human gut microbes associated with obesity. Nature 444(7122), 1022–1023. [PubMed: 17183309]

Lopez OL, Becker JT, Kuller LH, 2013 Patterns of compensation and vulnerability in normal subjects at risk of Alzheimer's disease. Journal of Alzheimer's disease : JAD 33 Suppl 1, S427–438. [PubMed: 22669014]

Macfabe DF, 2012 Short-chain fatty acid fermentation products of the gut microbiome: implications in autism spectrum disorders. Microb Ecol Health Dis 23.

Macfarlane S, Macfarlane GT, 2003 Regulation of short-chain fatty acid production. Proc Nutr Soc 62(1), 67–72. [PubMed: 12740060]

Madsen K, Cornish A, Soper P, McKaigney C, Jijon H, Yachimec C, Doyle J, Jewell L , De Simone C, 2001 Probiotic bacteria enhance murine and human intestinal epithelial barrier function. Gastroenterology 121(3), 580–591. [PubMed: 11522742]

Mano N, Goto T, Uchida M, Nishimura K, Ando M, Kobayashi N, Goto J, 2004 Presence of protein-bound unconjugated bile acids in the cytoplasmic fraction of rat brain. J Lipid Res 45(2), 295–300. [PubMed: 14617741]

Manocha GD, Floden AM, Miller NM, Smith AJ, Nagamoto-Combs K, Saito T, Saido TC, Combs CK, 2019 Temporal progression of Alzheimer's disease in brains and intestines of transgenic mice. Neurobiology of aging 81, 166–176. [PubMed: 31284126]

Mariat D, Firmesse O, Levenez F, Guimaraes V, Sokol H, Dore J, Corthier G, Furet JP, 2009 The Firmicutes/Bacteroidetes ratio of the human microbiota changes with age. BMC Microbiol 9, 123. [PubMed: 19508720]

Marksteiner J, Blasko I, Kemmler G, Koal T, Humpel C, 2018 Bile acid quantification of 20 plasma metabolites identifies lithocholic acid as a putative biomarker in Alzheimer's disease. Metabolomics 14(1), 1. [PubMed: 29249916]

McMillin M, DeMorrow S, 2016 Effects of bile acids on neurological function and disease. FASEB J 30(11), 3658–3668. [PubMed: 27468758]

Mendes MCS, Paulino DS, Brambilla SR, Camargo JA, Persinoti GF, Carvalheira JBC, 2018 Microbiota modification by probiotic supplementation reduces colitis associated colon cancer in mice. World J Gastroenterol 24(18), 1995–2008. [PubMed: 29760543]

Minter MR, Zhang C, Leone V, Ringus DL, Zhang X, Oyler-Castrillo P, Musch MW, Liao F, Ward JF, Holtzman DM, Chang EB, Tanzi RE, Sisodia SS, 2016 Antibiotic-induced perturbations in gut microbial diversity influences neuro-inflammation and amyloidosis in a murine model of Alzheimer's disease. Scientific reports 6, 30028. [PubMed: 27443609]

Author Manuscript Author Manuscript Author Manuscript Author Manuscript

Montonye DR, Ericsson AC, Busi SB, Lutz C, Wardwell K, Franklin CL, 2018 Acclimation and Institutionalization of the Mouse Microbiota Following Transportation. Frontiers in microbiology 9, 1085. [PubMed: 29892276]

Morales I, Guzman-Martinez L, Cerda-Troncoso C, Farias GA, Maccioni RB, 2014 Neuroinflammation in the pathogenesis of Alzheimer's disease. A rational framework for the search of novel therapeutic approaches. Front Cell Neurosci 8, 112. [PubMed: 24795567]

Moretti M, Valvassori SS, Varela RB, Ferreira CL, Rochi N, Benedet J, Scaini G, Kapczinski F, Streck EL, Zugno AI, Quevedo J, 2011 Behavioral and neurochemical effects of sodium butyrate in an animal model of mania. Behav Pharmacol 22(8), 766–772. [PubMed: 21989497]

Musso G, Gambino R, Cassader M, 2011 Interactions between gut microbiota and host metabolism predisposing to obesity and diabetes. Annu Rev Med 62, 361–380. [PubMed: 21226616]

Nagamoto-Combs K, Manocha GD, Puig K, Combs CK, 2016 An improved approach to align and embed multiple brain samples in a gelatin-based matrix for simultaneous histological processing. J Neurosci Methods 261, 155–160. [PubMed: 26743972]

Nguyen TT, Kosciolek T, Eyler LT, Knight R, Jeste DV, 2018 Overview and systematic review of studies of microbiome in schizophrenia and bipolar disorder. J Psychiatr Res 99, 50–61. [PubMed: 29407287]

Nimgampalle M, Kuna Y, 2017 Anti-Alzheimer Properties of Probiotic, Lactobacillus plantarum MTCC 1325 in Alzheimer's Disease induced Albino Rats. Journal of clinical and diagnostic research : JCDR 11(8), KC01–KC05.

Nunes AF, Amaral JD, Lo AC, Fonseca MB, Viana RJ, Callaerts-Vegh Z, D'Hooge R, Rodrigues CM, 2012 TUDCA, a bile acid, attenuates amyloid precursor protein processing and amyloid-beta deposition in APP/PS1 mice. Mol Neurobiol 45(3), 440–454. [PubMed: 22438081]

Ottman N, Davids M, Suarez-Diez M, Boeren S, Schaap PJ, Martins Dos Santos VAP, Smidt H, Belzer C, de Vos WM, 2017 Genome-Scale Model and Omics Analysis of Metabolic Capacities of Akkermansia muciniphila Reveal a Preferential Mucin-Degrading Lifestyle. Appl Environ Microbiol 83(18).

Pagnini C, Saeed R, Bamias G, Arseneau KO, Pizarro TT, Cominelli F, 2010 Probiotics promote gut health through stimulation of epithelial innate immunity. Proc Natl Acad Sci U S A 107(1), 454–459. [PubMed: 20018654]

Pan X, Elliott CT, McGuinness B, Passmore P, Kehoe PG, Holscher C, McClean PL, Graham SF, Green BD, 2017 Metabolomic Profiling of Bile Acids in Clinical and Experimental Samples of Alzheimer's Disease. Metabolites 7(2).

Park JY, Choi J, Lee Y, Lee JE, Lee EH, Kwon HJ, Yang J, Jeong BR, Kim YK, Han PL, 2017 Metagenome Analysis of Bodily Microbiota in a Mouse Model of Alzheimer Disease Using Bacteria-derived Membrane Vesicles in Blood. Exp Neurobiol 26(6), 369–379. [PubMed: 29302204]

Paveljsek D, Juvan P, Kosir R, Rozman D, Hacin B, Ivicak-Kocjan K, Rogelj I, 2018 Lactobacillus fermentum L930BB and Bifidobacterium animalis subsp. animalis IM386 initiate signalling pathways involved in intestinal epithelial barrier protection. Benef Microbes 9(3), 515–525. [PubMed: 29633647]

Pereira-Marques J, Hout A, Ferreira RM, Weber M, Pinto-Ribeiro I, van Doorn LJ, Knetsch CW, Figueiredo C, 2019 Impact of Host DNA and Sequencing Depth on the Taxonomic Resolution of Whole Metagenome Sequencing for Microbiome Analysis. Frontiers in microbiology 10, 1277. [PubMed: 31244801]

Pistollato F, Sumalla Cano S, Elio I, Masias Vergara M, Giampieri F, Battino M, 2016 Role of gut microbiota and nutrients in amyloid formation and pathogenesis of Alzheimer disease. Nutr Rev 74(10), 624–634. [PubMed: 27634977]

Plovier H, Everard A, Druart C, Depommier C, Van Hul M, Geurts L, Chilloux J, Ottman N, Duparc T, Lichtenstein L, Myridakis A, Delzenne NM, Klievink J, Bhattacharjee A, van der Ark KC, Aalvink S, Martinez LO, Dumas ME, Maiter D, Loumaye A, Hermans MP, Thissen JP, Belzer C, de Vos WM, Cani PD, 2017 A purified membrane protein from Akkermansia muciniphila or the pasteurized bacterium improves metabolism in obese and diabetic mice. Nat Med 23(1), 107–113. [PubMed: 27892954]

Author Manuscript Author Manuscript Author Manuscript Author Manuscript

Png CW, Linden SK, Gilshenan KS, Zoetendal EG, McSweeney CS, Sly LI, McGuckin MA, Florin TH, 2010 Mucolytic bacteria with increased prevalence in IBD mucosa augment in vitro utilization of mucin by other bacteria. Am J Gastroenterol 105(11), 2420–2428. [PubMed: 20648002]

Puig KL, Lutz BM, Urquhart SA, Rebel AA, Zhou X, Manocha GD, Sens M, Tuteja AK, Foster NL, Combs CK, 2015 Overexpression of mutant amyloid-beta protein precursor and presenilin 1 modulates enteric nervous system. Journal of Alzheimer's disease : JAD 44(4), 1263–1278. [PubMed: 25408221]

Qiu C, Fratiglioni L, 2018 Aging without Dementia is Achievable: Current Evidence from Epidemiological Research. Journal of Alzheimer's disease : JAD 62(3), 933–942. [PubMed: 29562544]

Quinn M, 2013 Bile in the Brain? A Role for Bile Acids in the Central Nervous System. Journal of Cell Science & Therapy 3(113).

Raatz SK, Golovko MY, Brose SA, Rosenberger TA, Burr GS, Wolters WR, Picklo MJ Sr., 2011 Baking reduces prostaglandin, resolvin, and hydroxy-fatty acid content of farm-raised Atlantic salmon (Salmo salar). J Agric Food Chem 59(20), 11278–11286. [PubMed: 21919483]

Rajilic-Stojanovic M, Shanahan F, Guarner F, de Vos WM, 2013 Phylogenetic analysis of dysbiosis in ulcerative colitis during remission. Inflamm Bowel Dis 19(3), 481–488. [PubMed: 23385241]

Reagan-Shaw S, Nihal M, Ahmad N, 2008 Dose translation from animal to human studies revisited. FASEB J 22(3), 659–661. [PubMed: 17942826]

Ridlon JM, Kang DJ, Hylemon PB, Bajaj JS, 2014 Bile acids and the gut microbiome. Curr Opin Gastroenterol 30(3), 332–338. [PubMed: 24625896]

Saito T, Matsuba Y, Mihira N, Takano J, Nilsson P, Itohara S, Iwata N, Saido TC, 2014 Single App knock-in mouse models of Alzheimer's disease. Nat Neurosci 17(5), 661–663. [PubMed: 24728269]

Sandman PO, Adolfsson R, Hallmans G, Nygren C, Nystrom L, Winblad B, 1983 Treatment of constipation with high-bran bread in long-term care of severely demented elderly patients. J Am Geriatr Soc 31(5), 289–293. [PubMed: 6302153]

Semar S, Klotz M, Letiembre M, Van Ginneken C, Braun A, Jost V, Bischof M, Lammers WJ, Liu Y, Fassbender K, Wyss-Coray T, Kirchhoff F, Schafer KH, 2013 Changes of the enteric nervous system in amyloid-beta protein precursor transgenic mice correlate with disease progression. Journal of Alzheimer's disease : JAD 36(1), 7–20. [PubMed: 23531500]

Sender R, Fuchs S, Milo R, 2016 Revised Estimates for the Number of Human and Bacteria Cells in the Body. PLoS biology 14(8), e1002533. [PubMed: 27541692]

Shen L, Liu L, Ji HF, 2017 Alzheimer's Disease Histological and Behavioral Manifestations in Transgenic Mice Correlate with Specific Gut Microbiome State. Journal of Alzheimer's disease : JAD 56(1), 385–390. [PubMed: 27911317]

Shibolet O, Karmeli F, Eliakim R, Swennen E, Brigidi P, Gionchetti P, Campieri M, Morgenstern S, Rachmilewitz D, 2002 Variable response to probiotics in two models of experimental colitis in rats. Inflamm Bowel Dis 8(6), 399–406. [PubMed: 12454615]

Sonnenberg A, Tsou VT, Muller AD, 1994 The "institutional colon": a frequent colonic dysmotility in psychiatric and neurologic disease. Am J Gastroenterol 89(1), 62–66. [PubMed: 8273800]

Sun D, Gu G, Wang J, Chai Y, Fan Y, Yang M, Xu X, Gao W, Li F, Yin D, Zhou S, Chen X, Zhang J, 2017 Administration of Tauroursodeoxycholic Acid Attenuates Early Brain Injury via Akt Pathway Activation. Front Cell Neurosci 11, 193. [PubMed: 28729823]

Swidsinski A, Dorffel Y, Loening-Baucke V, Theissig F, Ruckert JC, Ismail M, Rau WA, Gaschler D, Weizenegger M, Kuhn S, Schilling J, Dorffel WV, 2011 Acute appendicitis is characterised by local invasion with Fusobacterium nucleatum/necrophorum. Gut 60(1), 34–40. [PubMed: 19926616]

Theriot CM, Koenigsknecht MJ, Carlson PE Jr., Hatton GE, Nelson AM, Li B, Huffnagle GB, J ZL, Young VB, 2014 Antibiotic-induced shifts in the mouse gut microbiome and metabolome increase susceptibility to Clostridium difficile infection. Nat Commun 5, 3114. [PubMed: 24445449]

Tursi A, Brandimarte G, Papa A, Giglio A, Elisei W, Giorgetti GM, Forti G, Morini S, Hassan C, Pistoia MA, Modeo ME, Rodino S, D'Amico T, Sebkova L, Sacca N, Di Giulio E, Luzza F,

Author Manuscript Author Manuscript Author Manuscript Author Manuscript

Imeneo M, Larussa T, Di Rosa S, Annese V, Danese S, Gasbarrini A, 2010 Treatment of relapsing mild-to-moderate ulcerative colitis with the probiotic VSL#3 as adjunctive to a standard pharmaceutical treatment: a double-blind, randomized, placebo-controlled study. Am J Gastroenterol 105(10), 2218–2227. [PubMed: 20517305]

Uronis JM, Arthur JC, Keku T, Fodor A, Carroll IM, Cruz ML, Appleyard CB, Jobin C, 2011 Gut microbial diversity is reduced by the probiotic VSL#3 and correlates with decreased TNBS-induced colitis. Inflamm Bowel Dis 17(1), 289–297. [PubMed: 20564535]

Vecchione A, Celandroni F, Mazzantini D, Senesi S, Lupetti A, Ghelardi E, 2018 Compositional Quality and Potential Gastrointestinal Behavior of Probiotic Products Commercialized in Italy. Frontiers in medicine 5, 59. [PubMed: 29564327]

Vogt NM, Kerby RL, Dill-McFarland KA, Harding SJ, Merluzzi AP, Johnson SC, Carlsson CM, Asthana S, Zetterberg H, Blennow K, Bendlin BB, Rey FE, 2017 Gut microbiome alterations in Alzheimer's disease. Scientific reports 7(1), 13537. [PubMed: 29051531]

Wang CS, Li WB, Wang HY, Ma YM, Zhao XH, Yang H, Qian JM, Li JN, 2018 VSL#3 can prevent ulcerative colitis-associated carcinogenesis in mice. World J Gastroenterol 24(37), 4254–4262. [PubMed: 30310258]

Wang QJ, Shen YE, Wang X, Fu S, Zhang X, Zhang YN, Wang RT, 2020 Concomitant memantine and Lactobacillus plantarum treatment attenuates cognitive impairments in APP/PS1 mice. Aging 12(1), 628–649. [PubMed: 31907339]

Wu SC, Cao ZS, Chang KM, Juang JL, 2017 Intestinal microbial dysbiosis aggravates the progression of Alzheimer's disease in Drosophila. Nat Commun 8(1), 24. [PubMed: 28634323]

Yadav H, Lee JH, Lloyd J, Walter P, Rane SG, 2013 Beneficial metabolic effects of a probiotic via butyrate-induced GLP-1 hormone secretion. J Biol Chem 288(35), 25088–25097. [PubMed: 23836895]

Zakostelska Z, Kverka M, Klimesova K, Rossmann P, Mrazek J, Kopecny J, Hornova M, Srutkova D, Hudcovic T, Ridl J, Tlaskalova-Hogenova H, 2011 Lysate of probiotic Lactobacillus casei DN-114 001 ameliorates colitis by strengthening the gut barrier function and changing the gut microenvironment. PLoS One 6(11), e27961. [PubMed: 22132181]

Zareie M, Johnson-Henry K, Jury J, Yang PC, Ngan BY, McKay DM, Soderholm JD, Perdue MH, Sherman PM, 2006 Probiotics prevent bacterial translocation and improve intestinal barrier function in rats following chronic psychological stress. Gut 55(11), 1553–1560. [PubMed: 16638791]

Zhang L, Wang Y, Xiayu X, Shi C, Chen W, Song N, Fu X, Zhou R, Xu YF, Huang L, Zhu H, Han Y, Qin C, 2017 Altered Gut Microbiota in a Mouse Model of Alzheimer's Disease. Journal of Alzheimer's disease : JAD 60(4), 1241–1257. [PubMed: 29036812]

Zhang X, Shen D, Fang Z, Jie Z, Qiu X, Zhang C, Chen Y, Ji L, 2013 Human gut microbiota changes reveal the progression of glucose intolerance. PLoS One 8(8), e71108. [PubMed: 24013136]

Zmora N, Zilberman-Schapira G, Suez J, Mor U, Dori-Bachash M, Bashiardes S, Kotler E, Zur M, Regev-Lehavi D, Brik RB, Federici S, Cohen Y, Linevsky R, Rothschild D, Moor AE, Ben-Moshe S, Harmelin A, Itzkovitz S, Maharshak N, Shibolet O, Shapiro H, Pevsner-Fischer M, Sharon I, Halpern Z, Segal E, Elinav E, 2018 Personalized Gut Mucosal Colonization Resistance to Empiric Probiotics Is Associated with Unique Host and Microbiome Features. Cell 174(6), 1388–1405 e1321. [PubMed: 30193112]

Author Manuscript Author Manuscript Author Manuscript Author Manuscript

Highlights

- *App*$^{NL-G-F}$ demonstrated increased intestinal permeability correlating with dysbiosis
- *App*$^{NL-G-F}$ mice had altered serum bile acids and prostaglandins compared to controls
- Probiotic supplementation of *App*$^{NL-G-F}$ mice attenuated intestinal dysfunction
- Probiotic fed *App*$^{NL-G-F}$ mice had minimal changes in gliosis and plaque load
- There is potential for probiotic intervention in AD

Author Manuscript Author Manuscript Author Manuscript Author Manuscript

Verification

1. The authors have no actual or potential conflicts of interest to disclose.

2. This work was supported by funding from Alzheimer's Association Research fellowship, AARF-17-533143, a University of North Dakota (UND) Post-Doc Pilot Grant, the North Dakota Experimental Program to Stimulate Competitive Research (ND EPSCoR), UND0021228, and National Institutes of Health 5R01AG048993, 5P20GM113123, U54GM128729, and P20GM103442.

3. The data contained in the manuscript being submitted have not been previously published, are not submitted elsewhere, and will not be submitted elsewhere while under consideration at Neurobiology of Aging.

4. Animal use was approved by the University of North Dakota Institutional Animal Care and Use Committee Protocol 1709-1.

5. All authors have reviewed the contents of the manuscript being submitted, approve of its contents and validate the accuracy of the data.

Author Manuscript Author Manuscript Author Manuscript Author Manuscript

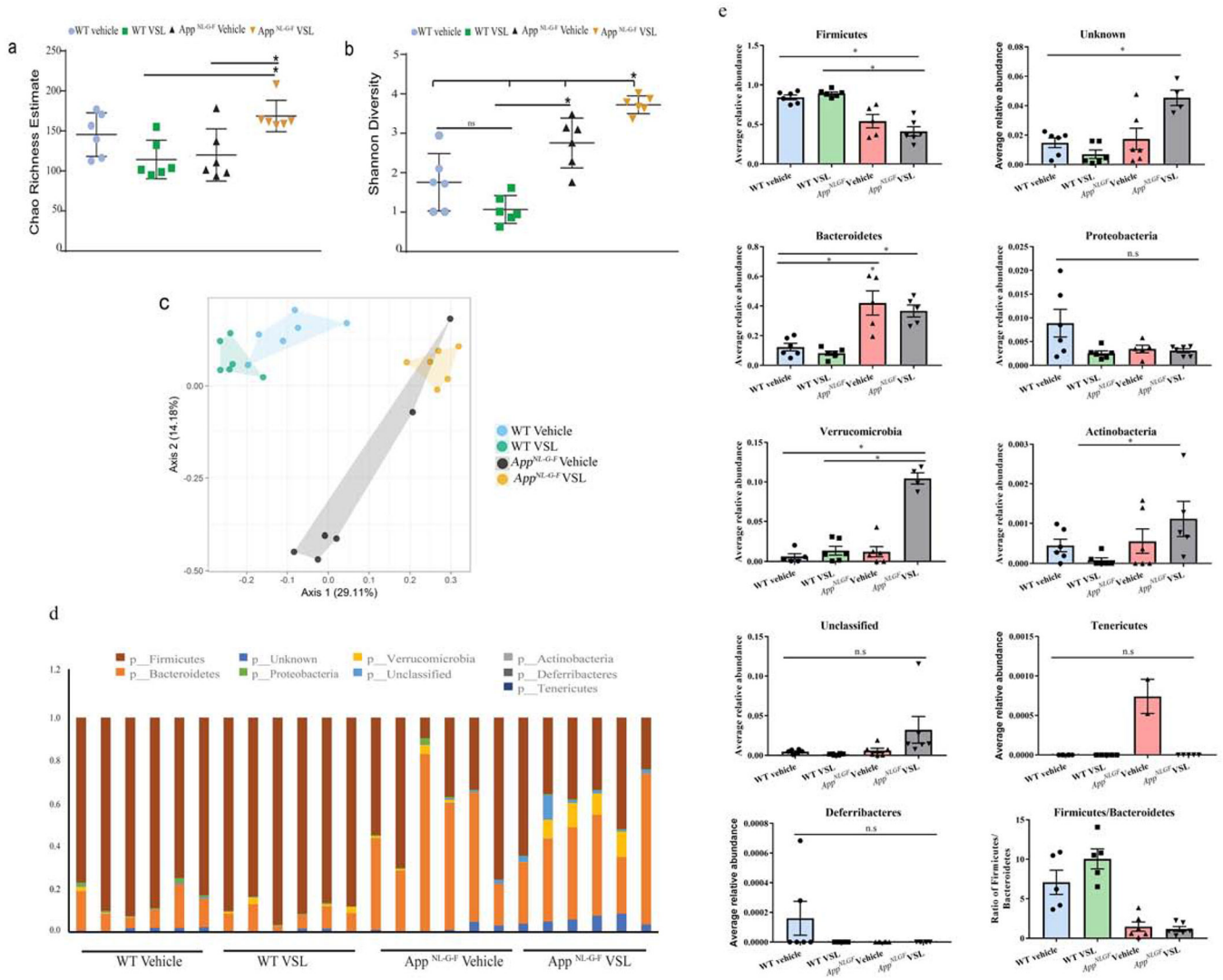

Fig. 1.

Gut bacterial phyla profile in *App*$^{NL\text{-}G\text{-}F}$ mice and effects of VSL#3 probiotic supplementation. Microbial richness was calculated based on Chao1 index (**a**) and microbial richness and evenness on the Shannon index (**b**). The mean value (and confidence interval) in each group are also illustrated (**c**). Principle coordinate analyses (PCoA) plot for unweighted UniFrac distances between C57BL/6 (WT) and *App*$^{NL\text{-}G\text{-}F}$ mice (**d**). Relative abundance of dominant bacterial phyla in fecal samples of C57BL/6 (WT) and *App*$^{NL\text{-}G\text{-}F}$ mice. The relative abundances are based on the proportional frequencies of the DNA sequences that were classified at the phylum level. 6 animals per group were examined (**e**) Each bar graphs shows the different bacterial phylum altered in *App*$^{NL\text{-}G\text{-}F}$ mice when compared to C57BL/6 (WT) vehicle treated mice. Data are represented as mean ± S.E.M. Significant differences were determined by two-way analysis of variance (ANOVA), * $p<0.05$ (n=6). The statistical analysis was not performed on phylum Deferribacteres and Tenericutes due to less average relative abundance of these phyla.

Author Manuscript Author Manuscript Author Manuscript Author Manuscript

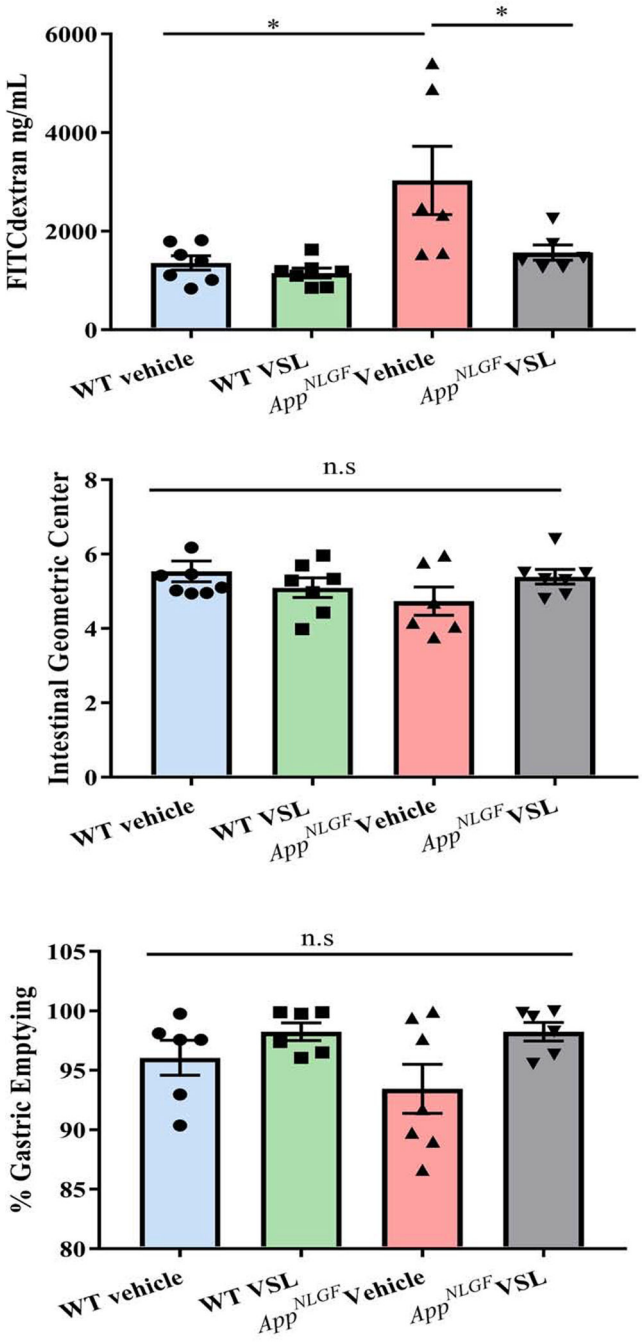

Fig. 2.

Effects of VSL#3 supplementation on intestinal permeability and motility in C57BL/6 (WT) and *App*$^{NL\text{-}G\text{-}F}$ mice. Permeability and motility assays were performed on C57BL/6 (WT) and *App*$^{NL\text{-}G\text{-}F}$ mice following 8 weeks of vehicle or VSL#3 supplementation. (**a**) Concentration of 4kDa FITC-conjugated dextran in serum as measured after 5 hours of oral gavage. To quantify motility mice were gavaged with 70 kDa FITC-conjugated dextran and (**b**) percentage gastric emptying and (**c**) intestinal transit were determined by assessing the dextran distribution throughout the gastrointestinal tract after 30 min. Data are represented

as mean ± S.E.M. Significant differences were determined by two-way ANOVA, * $p<0.05$ (n=7 and outlier removal resulted in statistical analysis from n=6-7).

Author Manuscript Author Manuscript Author Manuscript Author Manuscript

Author Manuscript Author Manuscript Author Manuscript Author Manuscript

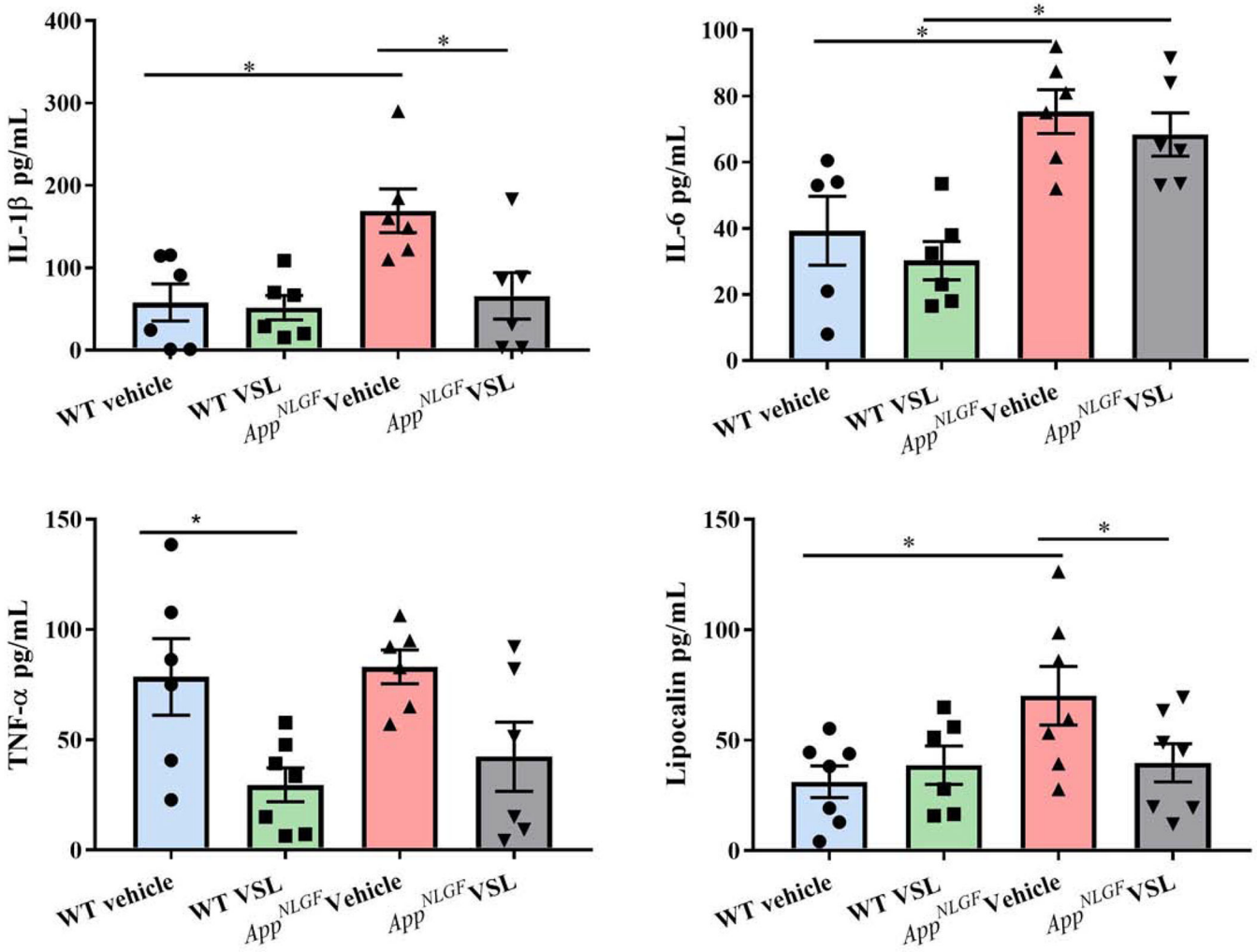

Fig. 3.

Effect of VSL#3 supplementation on pro-inflammatory cytokines and lipocalin (LCN-2) in ileums of C57BL/6 (WT) and *App*$^{NL\text{-}G\text{-}F}$ mice. Protein levels of (**a**) interleukin-1β (IL-1β), (**b**) IL-6, (**c**) tumor necrosis factor (TNF-α), and (**d**) lipocalin (LCN-2) levels were quantified from lysate prepared form ileums of vehicle and VSL#3 supplemented mice by enzyme-linked immunosorbent assay (ELISA). Data are represented as mean ± S.E.M. Significant differences were determined by two-way ANOVA, * $p<0.05$ (n=7 and outlier removal resulted in statistical analysis from n=6-7).

Author Manuscript Author Manuscript Author Manuscript Author Manuscript

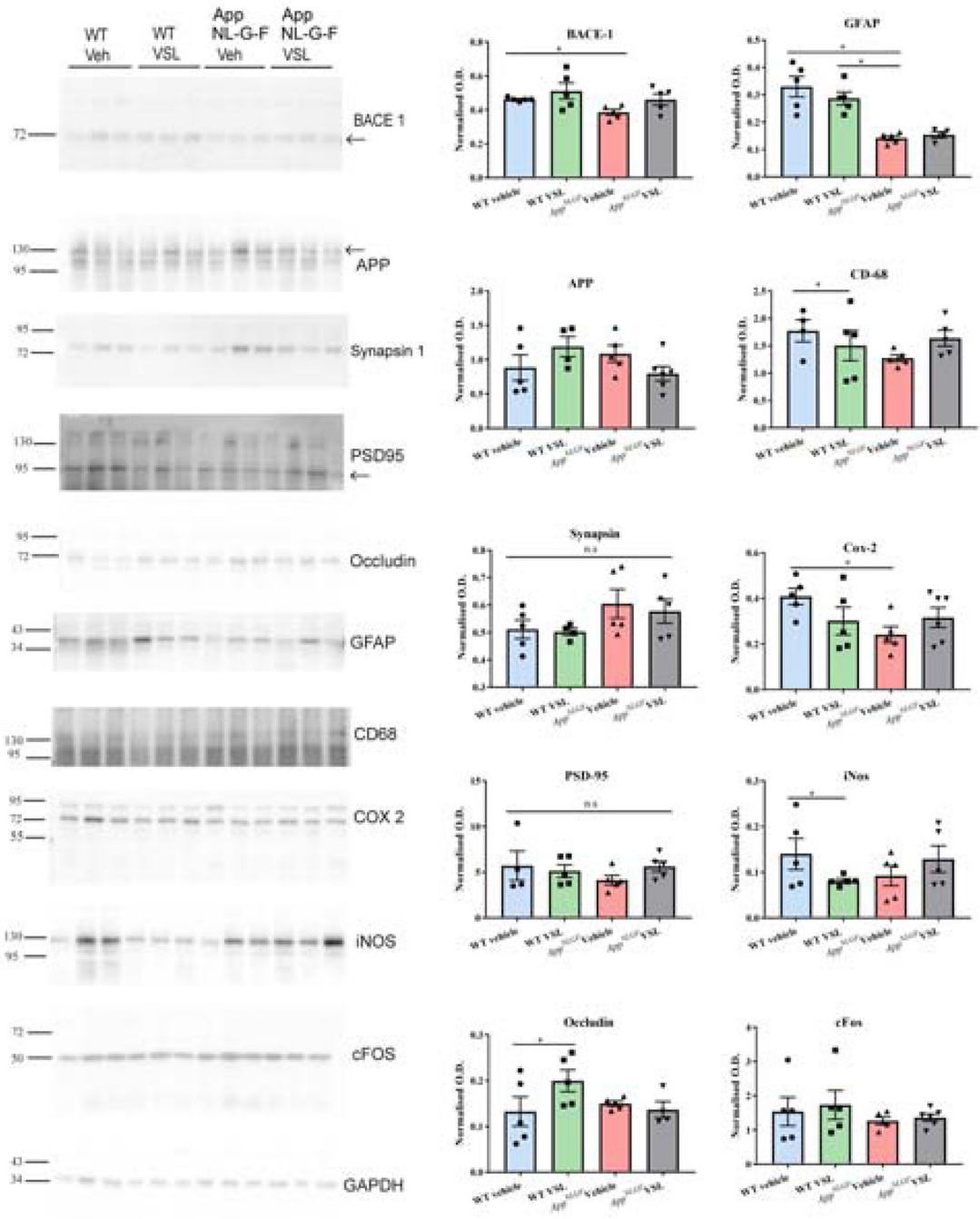

Fig. 4.

Effect of VSL#3 supplementation on inflammatory and tight junction proteins in ileums of C57BL/6 (WT) and *App*$^{NL\text{-}G\text{-}F}$ mice. Ileums from the mice were lysed and resolved via SDS-PAGE and western blotted using anti-BACE, anti-GFAP, anti-Iba-1, anti-APP, anti-CD-68, anti-synapsin-1, anti-Cox-2, anti-PSD-95, anti-iNOS, anti-cFos, anti-occludin and anti-GAPDH antibodies. Three representative western blots from 6 animals analyzed are shown in the figure. Quantification shows arbitrary densitometry units of each protein signal

normalized to its respective GAPDH loading control. Data are represented as mean ± S.E.M. Significant differences were determined by two-way analysis ANOVA, * $p<0.05$.

Author Manuscript Author Manuscript Author Manuscript Author Manuscript

Author Manuscript Author Manuscript Author Manuscript Author Manuscript

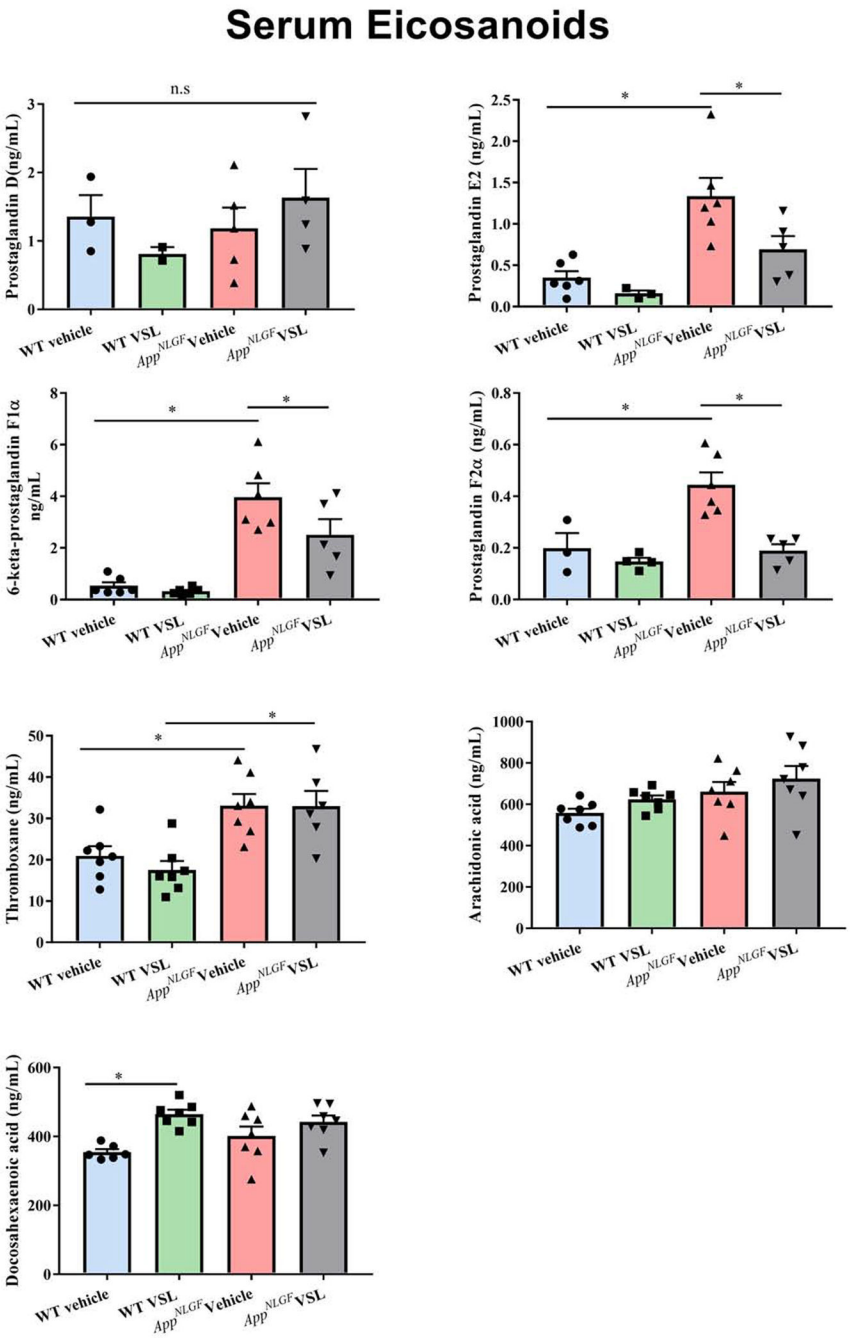

Fig. 5.

Effect of VSL#3 supplementation on serum concentrations of eicosanoids in C57BL/6 (WT) and *App*$^{NL\text{-}G\text{-}F}$ mice. (a) PGD_2 (b) PGE_2 (**c**) 6-keto $PGF_{1\alpha}$ (**d**) $PGF_{2\alpha}$ (**e**) thromboxane (**f**) arachidonic acid (Raatz et al.) (**g**) docosahexaenoic acid were measured by mass spectrometry in serum collected following 8 weeks of probiotic supplementation. Data are represented as mean ± S.E.M. Significant differences were determined by two-way ANOVA, * $p<0.05$ (n=7). Prostaglandin D was below the limit of detection (LOD) in several samples so statistical analysis was not performed on this analyte.

Author Manuscript
Author Manuscript
Author Manuscript
Author Manuscript

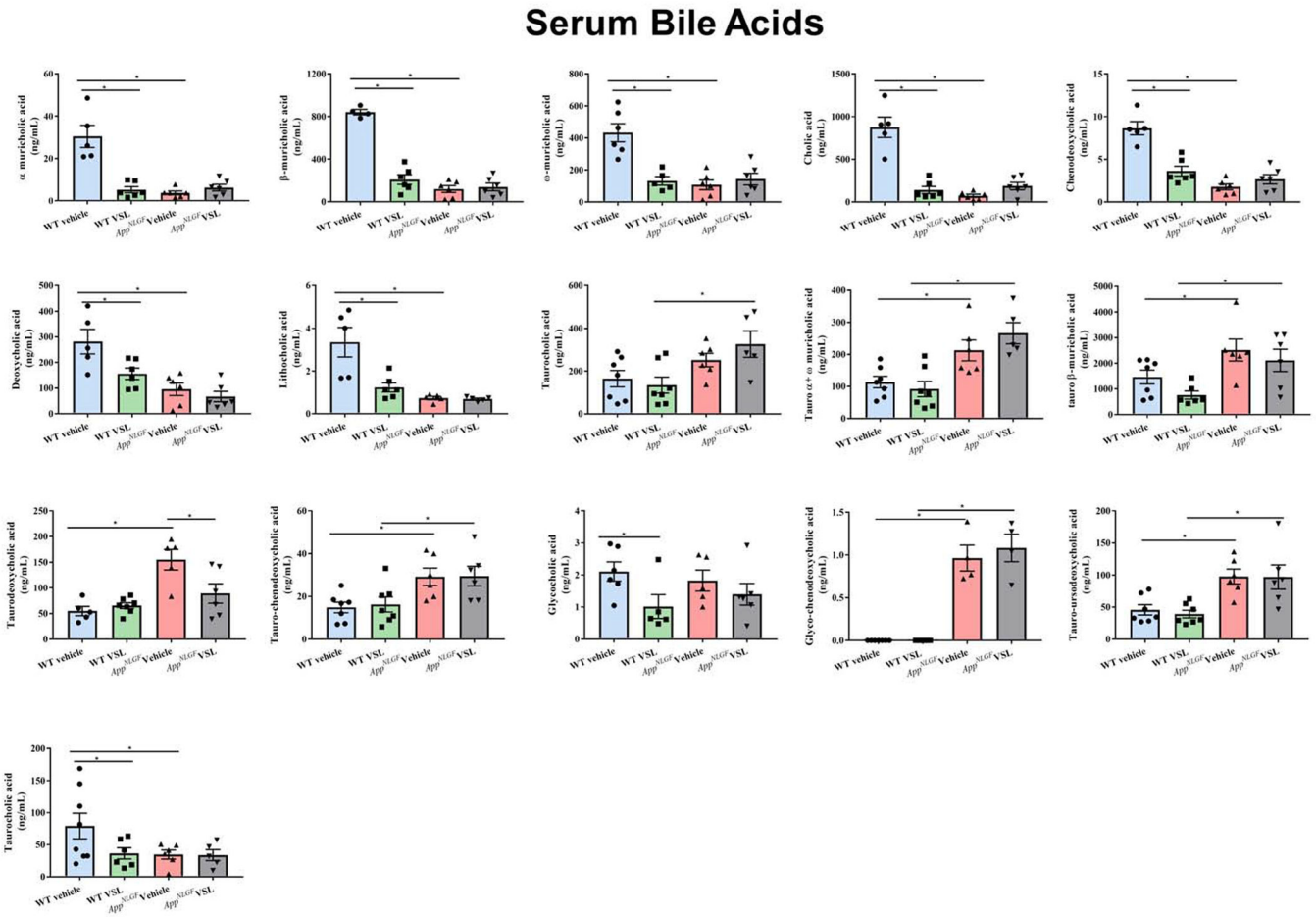

Fig. 6.

Effect of VSL#3 supplementation on different serum bile acid concentrations. Both conjugated and unconjugated primary and secondary bile acids (cholic, chenodeoxycholic acid, muricholic acid, deoxycholic acid, lithocholic acid) were estimated in serum samples using mass spectrometry. Data are represented as mean ± S.E.M. Significant differences were determined by two-way ANOVA, * $p<0.05$ (n=7).

Author Manuscript Author Manuscript Author Manuscript Author Manuscript

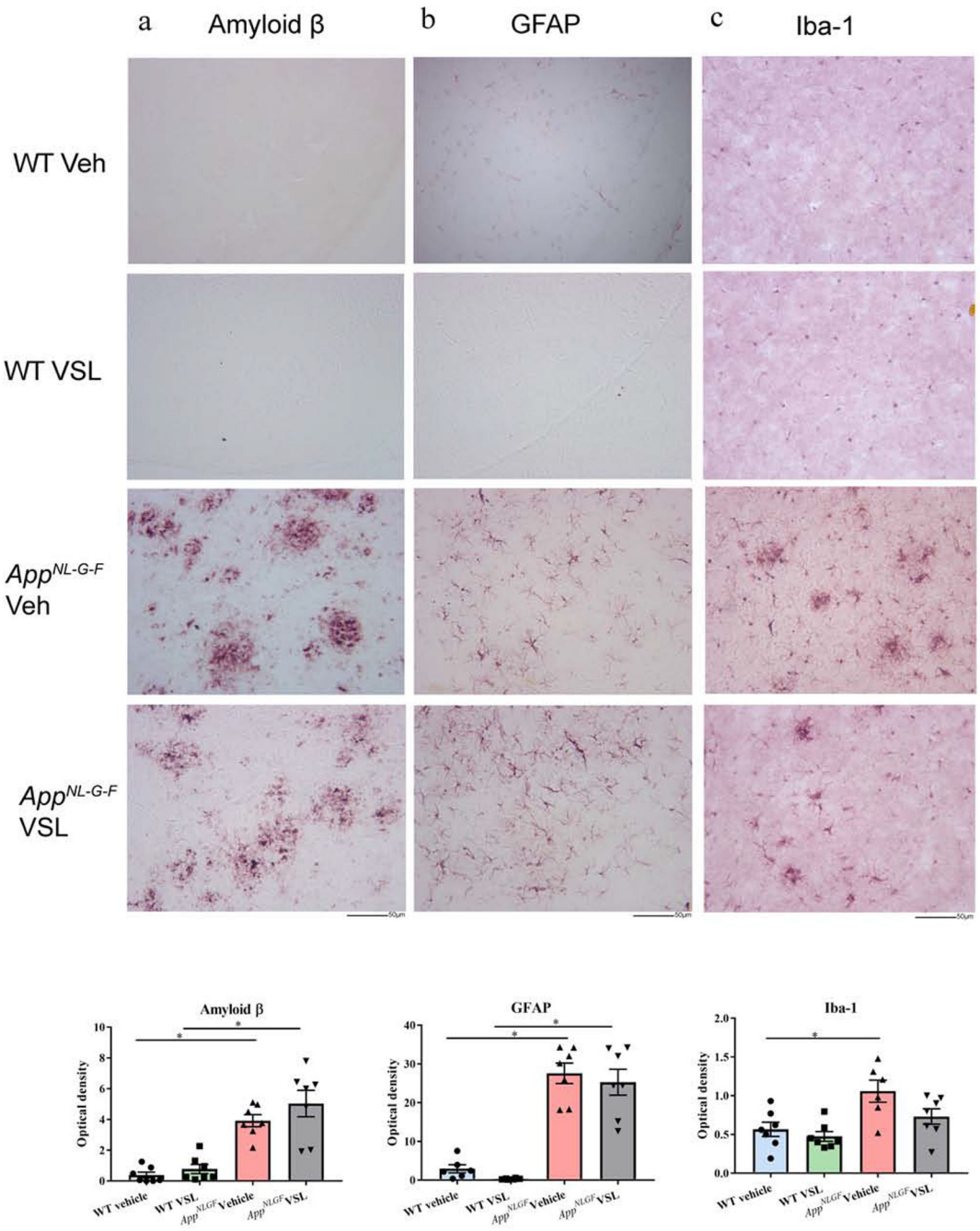

Fig. 7.

Effect of VSL#3 supplementation on Aβ accumulation and gliosis in brains of C57BL/6 (WT) and *App*$^{NL-G-F}$ mice. Representative immunohistochemical staining for (**a**) Aβ (**b**) GFAP, and (**c**) Iba-1 are shown from temporal cortex. The representative images shown were taken at 20x. Quantitation of immunostaining was performed, and optical density values were averaged and shown in bar graphs. Data are represented as mean ± S.E.M. Significant differences were determined by two-way ANOVA, * $p<0.05$ (n=7), Scale bar 50μm.

Author Manuscript Author Manuscript Author Manuscript Author Manuscript

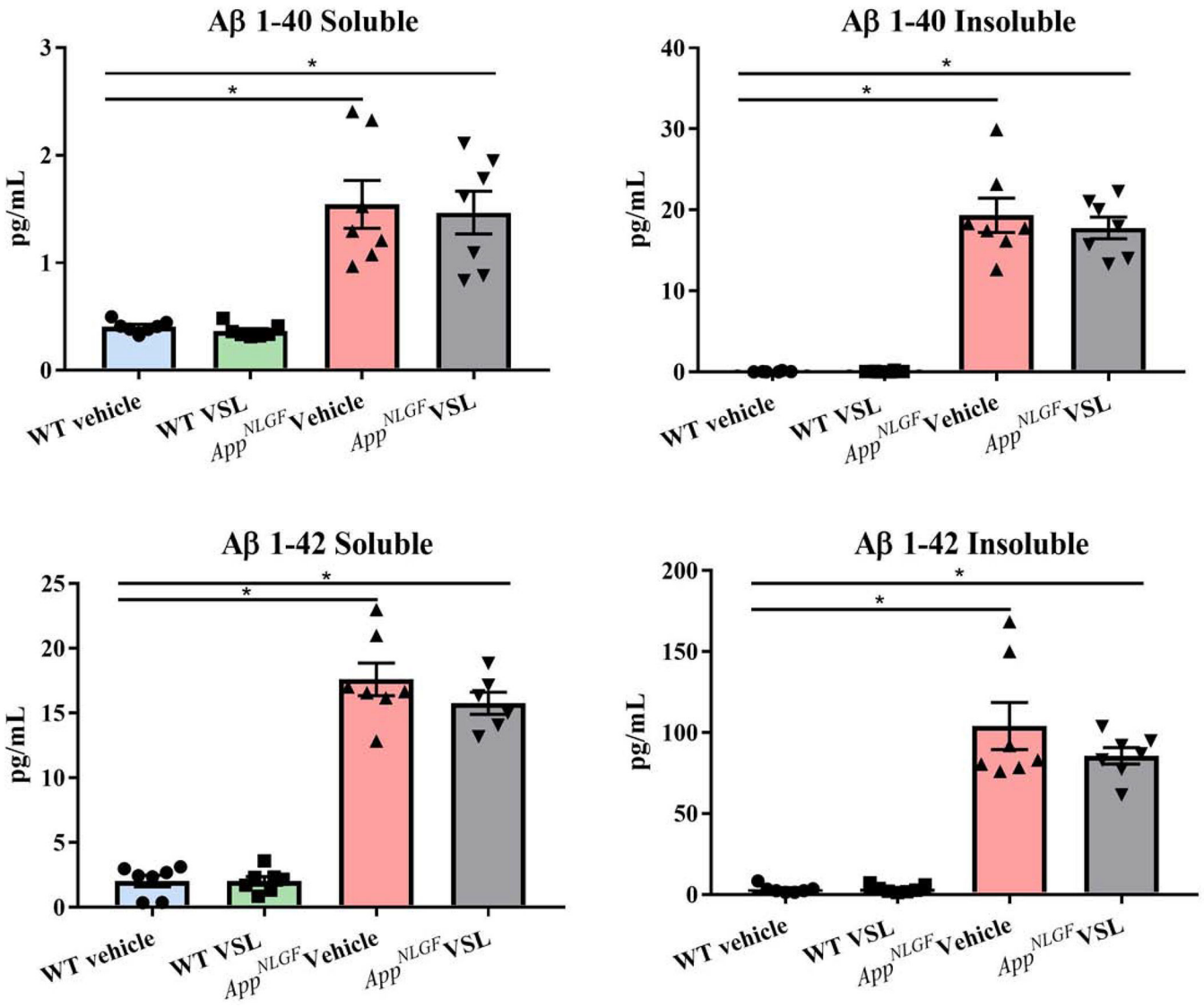

Fig. 8.

Effect of VSL#3 supplementation on brain Aβ levels. The levels of amyloid-beta 1-40 (Aβ 1-40) and 1-42 (Aβ 1-42), both soluble and insoluble, were assessed in temporal cortices of C57BL/6 (WT) and *App*$^{NL\text{-}G\text{-}F}$ mice using enzyme-linked immunosorbent assay (ELISA). 7 animals per group were examined. Data are represented as mean ± S.E.M. Significant differences were determined by two-way ANOVA, * $p<0.05$.

Author Manuscript Author Manuscript Author Manuscript Author Manuscript

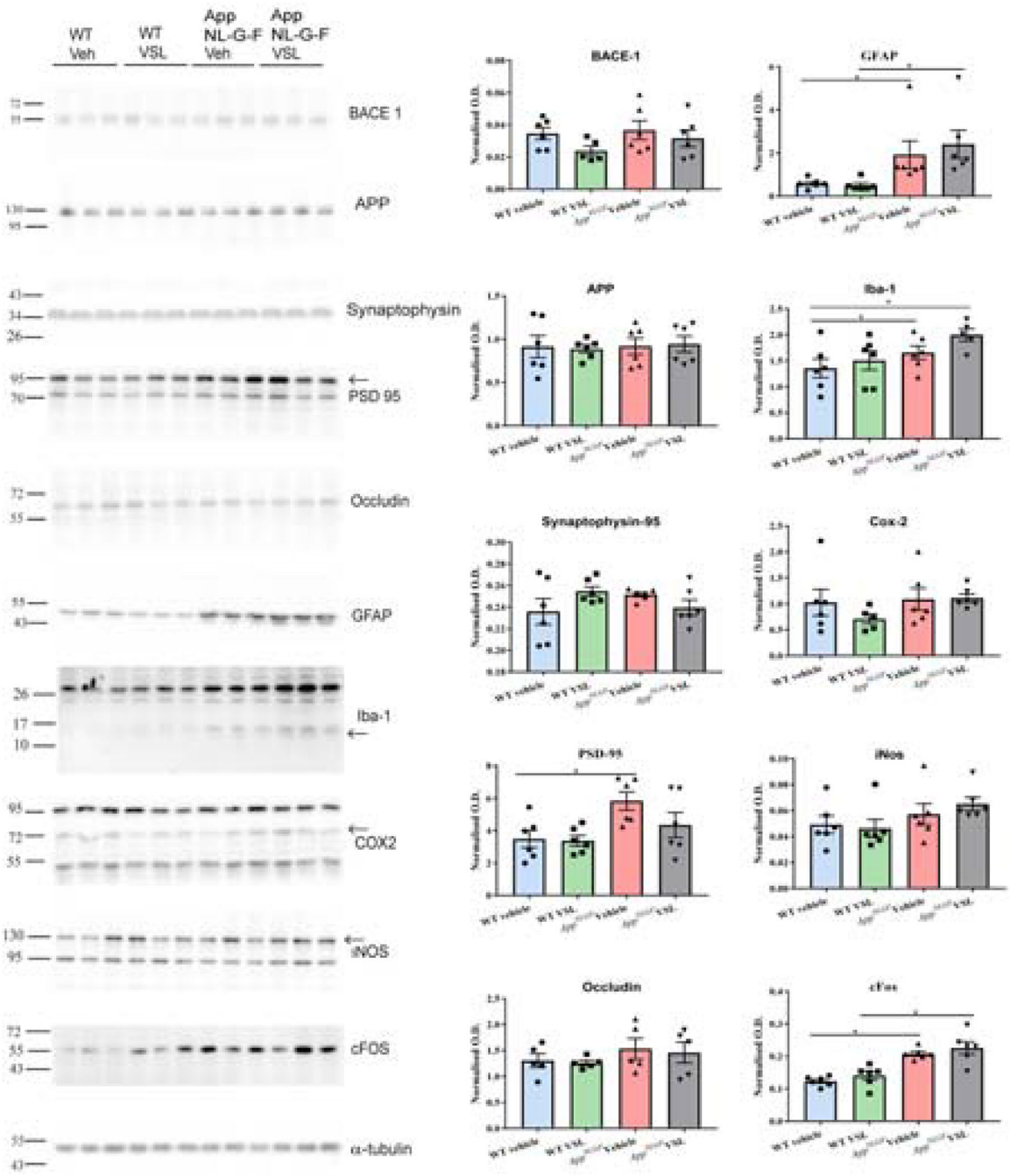

Fig. 9.

Effect of VSL#3 supplementation on different inflammatory proteins and a neuronal activity marker in the temporal cortex. The levels of inflammatory proteins, GFAP and Iba-1, along with neuronal activity marker protein, cFos, and post-synaptic protein PSD-95 were measured in temporal cortex lysates. Three representative western blots from 6 animals analyzed per group are shown with α-tubulin used as a loading control. Quantification shows arbitrary densitometry units of each protein signal normalized to α-tubulin. Data are

represented as mean ± S.E.M. Significant differences were determined by two-way ANOVA, * $p<0.05$.

Author Manuscript Author Manuscript Author Manuscript Author Manuscript

Author Manuscript Author Manuscript Author Manuscript Author Manuscript

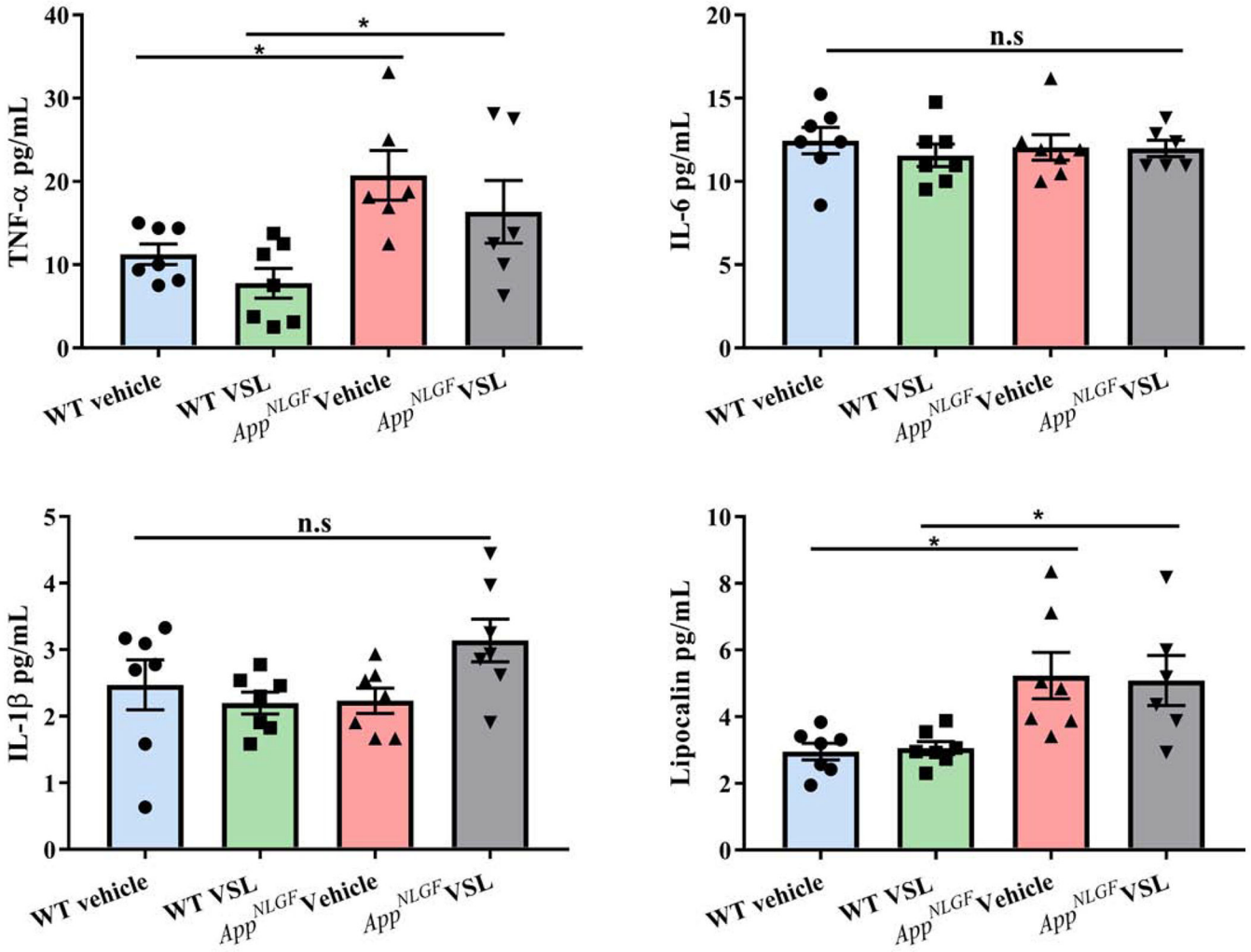

Fig. 10.

Effect of VSL#3 supplementation on pro-inflammatory cytokines in brains of C57BL/6 (WT) and *App*$^{NL\text{-}G\text{-}F}$ mice. Protein levels of (**a**) interleukin-1β (IL-1β), (**b**) IL-6, (**c**) tumor necrosis factor (TNF-α), and (**d**) lipocalin (LCN-2) from temporal cortices were examined by enzyme-linked immunosorbent assay (ELISA). (n=7 and outlier removal resulted in statistical analysis from n=6-7). Data are represented as mean ± S.E.M. Significant differences were determined by two-way ANOVA, * $p<0.05$.

Author Manuscript Author Manuscript Author Manuscript Author Manuscript

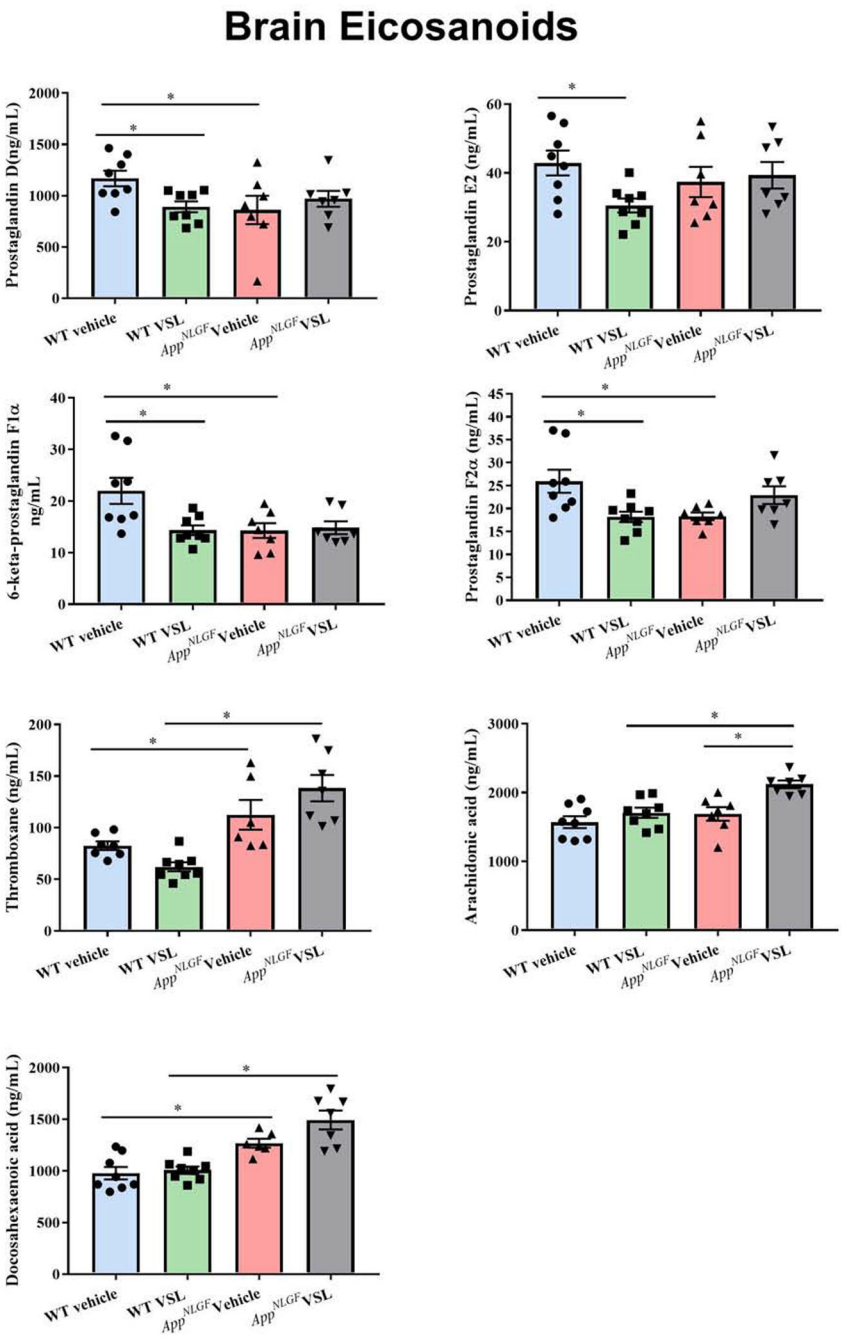

Fig. 11.

Effect of VSL#3 supplementation on brain concentrations of eicosanoids in C57BL/6 (WT) and *App*$^{NL\text{-}G\text{-}F}$ mice. (**a**) PGD, (**b**) PGE_2, (**c**) 6-keto $PGF_{1\alpha}$, (**d**) $PGF_{2\alpha}$, (**e**) thromboxane, (**f**) Arachidonic acid, and (**g**) Docosahexaenoic acid were measured using mass spectrometry in temporal cortices after 8 weeks of treatment. Data are represented as mean ± S.E.M. Significant differences were determined by two-way ANOVA, * $p<0.05$ (n=7 for *App*$^{NL\text{-}G\text{-}F}$ mice and n=8 for WT mice).

Author Manuscript Author Manuscript Author Manuscript Author Manuscript

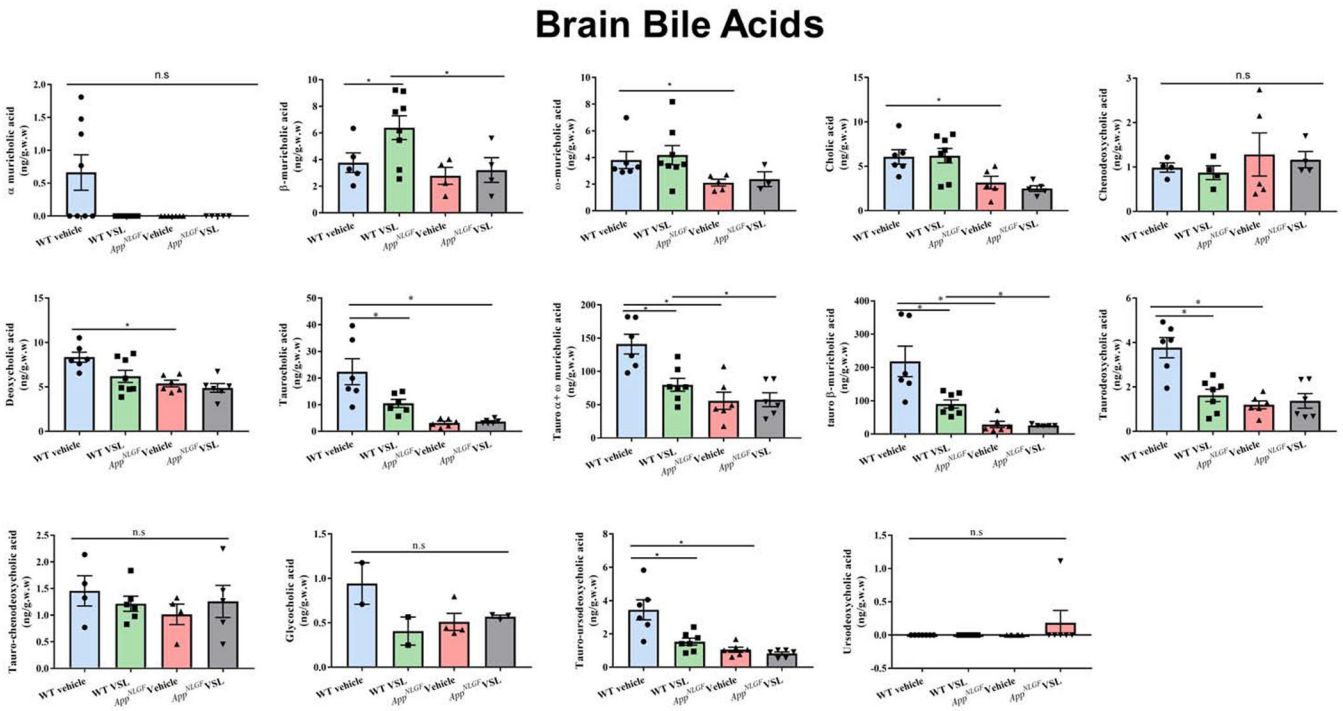

Fig. 12.

Effect of VSL#3 supplementation on bile acid concentrations in the brain. Both conjugated and unconjugated primary and secondary bile acids (cholic, chenodeoxycholic acid, muricholic acid, deoxycholic acid, lithocholic acid) were estimated in temporal cortex using mass spectrometry. Data are represented as mean ± S.E.M. Significant differences were determined by two-way ANOVA, * $p<0.05$ (n=7 for $App^{NL\text{-}G\text{-}F}$ mice and n=8 for WT mice). For bile acid levels found below the LOD such as α-muricholic acid, glycocholic acid, ursodeoxycholic acid, statistical analysis was not performed.

Author Manuscript Author Manuscript Author Manuscript Author Manuscript

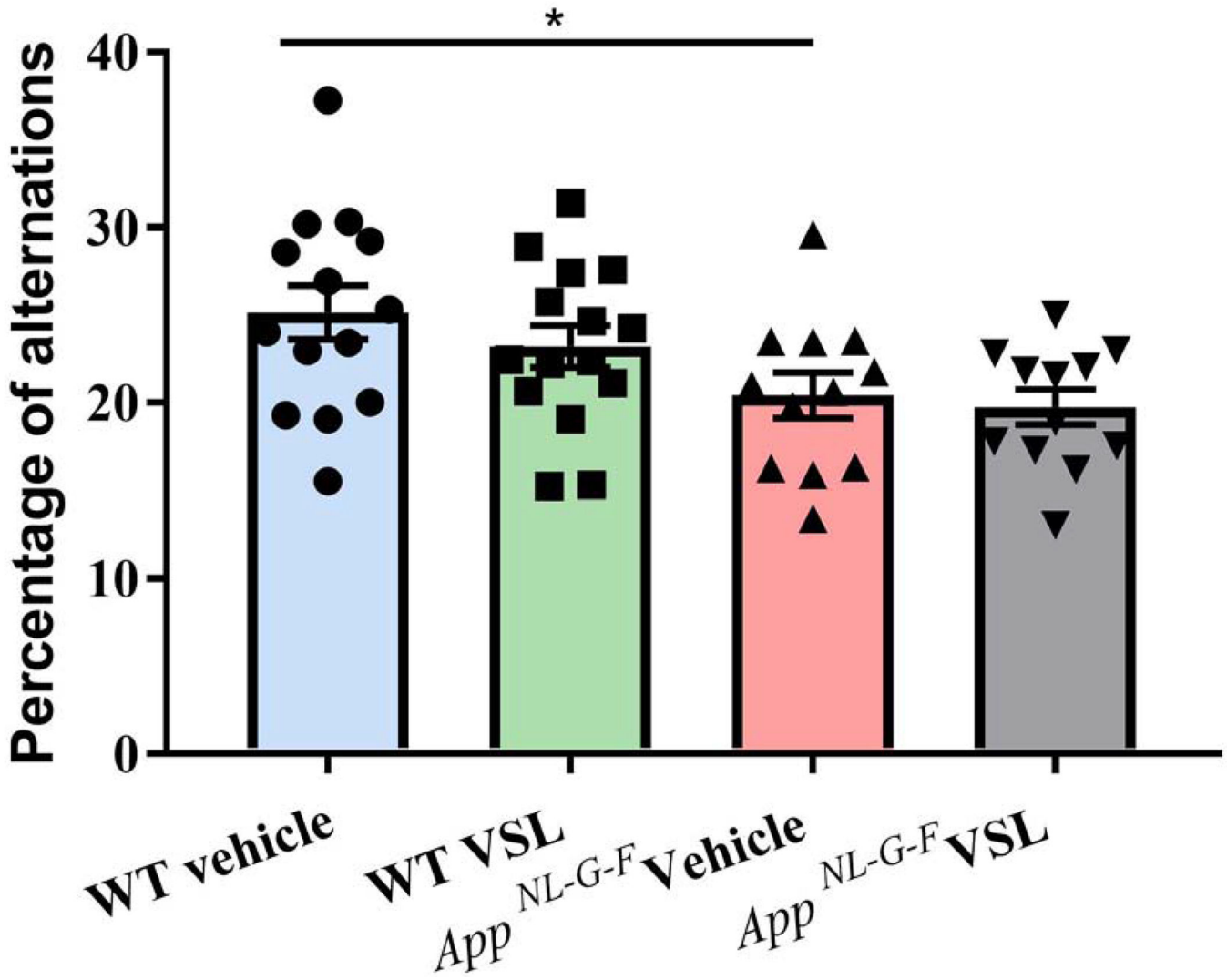

Fig.13.

Effect of VSL#3 supplementation on memory in C57BL/6 (WT) and *App*$^{NL\text{-}G\text{-}F}$ mice. All mice were subjected to cross maze testing for working memory after 8 weeks of treatment and the percentage of alternation were calculated and plotted. Data are represented as mean ± S.E.M. Significant differences were determined by two-way ANOVA, * $p<0.05$ (n=15). Mice that made fewer than 12 choices in an alternation task were excluded from the analysis.